UNIVERSITAS INDONESIA

MODELLING SIZE EFFECT IN CONCRETE SPECIMEN

TESIS

ANNIE WULANDARI
0806423330

FAKULTAS TEKNIK
PROGRAM TEKNIK SIPIL
JAKARTA
AGUSTUS 2010

UNIVERSITAS INDONESIA

MODELLING SIZE EFFECT IN CONCRETE SPECIMEN

TESIS

Diajukan sebagai salah satu syarat untuk memperoleh gelar Master Teknik

ANNIE WULANDARI
0806423330

FAKULTAS TEKNIK
PROGRAM TEKNIK SIPIL
KEKHUSUSAN STRUKTUR
JAKARTA
AGUSTUS 2010

HALAMAN PERNYATAAN ORISINALITAS

Tesis ini adalah hasil karya saya sendiri,
dan semua sumber baik yang dikutip maupun dirujuk
telah saya nyatakan dengan benar.

Nama	: Annie Wulandari
NPM	: 080642330
Tanda Tangan	:
Tanggal	: Agustus 2010

HALAMAN PENGESAHAN

Tesis ini diajukan oleh :
Nama : Annie Wulandari
NPM : 0806423330
Program Studi : Teknik Sipil
Judul Skripsi : Modelling Size Effect in Concrete Specimen

Telah berhasil dipertahankan di hadapan Dewan Penguji dan diterima sebagai
bagian persyaratan yang diperlukan untuk memperoleh gelar Magister Teknik pada Program Studi Teknik Sipil, Fakultas Teknik, Universitas Indonesia

DEWAN PENGUJI
Pembimbing : Prof. Panagiotis Kotronis
Pembimbing : Syed Yasir Alam
Ditetapkan di : Nantes
Tanggal : Juli 2010

ACKNOWLEDGEMENTS

The author acknowledges gratefully to

Panagiotis Kotronis
Syed Yasir-Alam

as supervisors whose encouragement, guidance and support from the initial to the final level enabled me to develop an understanding of the subject.

For my family

Thank you for the supports

HALAMAN PERNYATAAN PERSETUJUAN PUBLIKASI
TUGAS AKHIR UNTUK KEPENTINGAN AKADEMIS

Sebagai sivitas akademik Universitas Indonesia, saya yang bertanda tangan di bawah ini:

Nama : Annie Wulandari
NPM : 0806423330
Program Studi : Teknik Sipil
Departemen : Teknik Sipil
Fakultas : Teknik
Jenis karya : Tesis

demi pengembangan ilmu pengetahuan, menyetujui untuk memberikan kepada Universitas Indonesia **Hak Bebas Royalti Noneksklusif (*Non-exclusive Royalty-Free Right*)** atas karya ilmiah saya yang berjudul :

Modelling Size Effect in Concrete Specimen

beserta perangkat yang ada (jika diperlukan). Dengan Hak Bebas Royalti Noneksklusif ini Universitas Indonesia berhak menyimpan, mengalihmedia/formatkan, mengelola dalam bentuk pangkalan data (*database*), merawat, dan memublikasikan tugas akhir saya selama tetap mencantumkan nama saya sebagai penulis/pencipta dan sebagai pemilik Hak Cipta.

Demikian pernyataan ini saya buat dengan sebenarnya.

Dibuat di : Jakarta
Pada tanggal : 28 Mei 2011
Yang menyatakan

(……)

ABSTRACT

Name : Annie Wulandari
Study Program : Civil Engineering
Title : Modelling Size Effect in Concrete Specimen

Size effect on structural strength is normally understood as the effect of the characteristic structure size on the nominal strength of the structure when geometrically similar structures are compared. Fracture test are usually conducted on relatively small specimen and them this information is extrapolated to large structures. The question is that are we able to reproduce the size effect in the modern numerical techniques. Numerical calculations by computational code based on finite element have been done. The results show that in order to produce a size effect, it is necessary to use a regularization method.

Key words :
concrete, size effect, damage, regularization method

DAFTAR ISI

LIST OF FIGURES

List of Tables

CHAPTER 1
INTRODUCTION

The study of propagation of cracks in concrete elements of structures is considered important since it influences the ultimate strength and the resistance of a structure. One of the approaches that can be used to analyze this crack propagation is by Continuum Damage Mechanics. Continuum damage mechanics approach allows one to describe the material damage, from an undamaged state to its final state, corresponding to the macrocrack initiation and propagation. Throughout the years, different concepts involving continuum damage mechanics have been used to simulate the experimentally observed behavior of concrete materials. Many researchers applied continuum damage mechanics to linear elastic analysis of concrete where the mechanical effect of the progressive microcracking and strain softening are represented by a set of internal state variables which act on the elastic behavior (Mazars, 1984; Mazars and Pijaudier-Cabot, 1989; Willam et. al., 2001; Comi and Perego, 2001; Tao and Phillips, 2005; Labadi and Hannachi, 2005; Junior and Venturini, 2007; Khan et. al., 2007). One of the model, which is the model behavior of MAZARS[1] is a simple model based on the damage mechanics[2], which makes it possible to describe the decrease of material under the effect of the microcracks propagation in concrete. It relies on a single internal scalar variable D, describing the damage isotropically, but still distinguishing the damage of traction and compression.

Meanwhile, the study of structural strength cannot be separated from the scaling problem, especially on the quassibrittle materials, where these materials are incapable of fracture yielding, failing due to fracture that is characterized by a large fracture process zone[3]. Considering any type of geometrically similar specimens or structures of various sizes as shown in figure 1.1, with geometrically similar cracks, and plot the logarithm of the nominal stress σ_N versus logarithm of size. The strength criterion predicts σ_N at failure to be independent of size, while all tests indicate a decrease of σ_N with an increase of size. According to the classical linear fracture mechanics, σ_N in figure I.1 is then proportional to $(\text{size})^{-1/2}$. However with the exception of very large structures, this slope appears to be too

steep in comparison with most existing data. The reality seems to be a gradual transition from the horizontal straight line for the strength criterion to the inclined straight line of slope – ½. An analytical study of the size effect due to localization of distributed cracking was begun in 1976[4]. Later, a simple formula for the size effect, which describes the size effect for quasibrittle failures preceded by large stable crack growth and allows determination of material fracture parameters from maximum load tests, was derived[5] and the crack band model[6] was developed.

Figure 1. 1. Illustration of structural size effect in failure

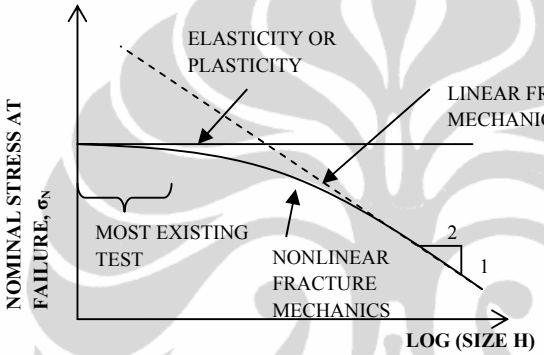

With an approach of a crack in a smeared manner, it is convenient to model the concrete in large finite element programs since its convenience in computational work as well as resemblance to reality. In this approach, introduced by Rashid (1968), many parallel cracks of infinitely small opening are imagined to be continuously distributed (smeared) over the finite elements. This can be conveniently modeled by reducing the material stiffness and strength in the direction normal to the cracks after the peak strength of the material has been reached. The evolution of the cracking process down to full fracture implies strain softening, a term which describes the post-peak gradual decline of stress at increasing strain. However, the smeared cracking approach leads to certain theoretical difficulties. They consist of the localization instabilities and spurious mesh sensitivity of finite element calculation. Therefore, one must seek an appropriate model to overcome the problem of mesh independency.

Regularization of fracture energy, which is introduced by La Borderie[7] and Hillerborg[8] is generally considered as a useful method to overcome this problem.

The main objective of this thesis is show whether it is possible to simulate size effect by using the modern regularization numerical methods; i.e is to seek the correlation between damage models, the crack concept along with the computational aspect implanted in the computer code based on finite element method. To understand the problem, the computation on this thesis will be divided into two models, a simple one dimensional concrete bar and a three point bending test of a concrete beam.

The second chapter on this thesis report will contain the theoretical approach which is the main basic of the numerical analysis that will be done. In this chapter, a brief explanation about smeared crack theory, as the concept used in the numerical analysis, will be presented. In this chapter also, the basic concept of scaling effect based on the crack band theory will be explained.

On the third chapter, the modeling techniques that the author will implement during the numerical analysis will be explained. This include the basic theory of Mazars law, the Hillerborg approach for regularization of mesh independency, and the La Borderie approach for crack propagation.

The fourth chapter will describe the numerical studies that the author has done. The first model is a one dimension concrete bar with a size of $0.1m \times 1m$, imposed by uniaxial force in the horizontal (x) direction. The damage model that will be used is the Mazar damage law, while the computational is done several approaches, i.e. local calculation, non-local calculation, the using of the Hillerborg[7] to obtain the regularization and La Borderie[8] method to validate the crack opening. To obtain the result regarding to the mesh dependency, the concrete is modeled in four different types of meshes, i.e. 11, 21, 31 and 61 meshes. The second model is the three point bending test, where a beam is considered to be imposed by a single load in the center of the beam. In order to seek the size effect, there will be three different size of concrete beams, i.e. $D_1 = 0{,}4m \times 0{,}1m$, $D_2 = 0{,}8m \times 0{,}2m$, and $D_3 = 1{,}6m \times 0{,}4m$. For the reason of simplicity, beams will be modeled only half of them. Using the Mazars damage

law, concrete is analyzed by two types of apporach, which are the non-local calculation and the Hillerborg method.

The result of the numerical studies will be presented in the fourth chapter. In the end of the chapter, the numerical result will be compared with the experimental result done by SYED Yasir Alam (2009).

In the last chapter of this thesis report, the main conclusion and notes for future work will be discussed.

CHAPTER 2
THEORITICAL APPROACH

2. 1. CRACK BAND THEORY

Basically, the concept of crack can be categorized into two; discrete concepts and smeared concepts. The former approach models a crack as a geometrical discontinuity, whereas the latter imagines a cracked solid to be a continuum. In the early days of finite element analysis cracks were modeled by means of a separation between element edges[9] . The approach suffers from two drawbacks. First, it implies a continuous change in nodal connectivity, which does not fit the nature of the finite element displacement method. Secondly, the crack is constrained to follow a predefined path along the element edges, which puts doubts on the fidelity of the approach.

The counterpart of the discrete crack concept is the smeared crack concept, in which a cracked solid is imagined to be a continuum. The approach, introduced by Rashid[10], starts from the notion of stress and strain and permits a description in terms of stress-strain relations. The procedure is attractive not only because it preserves the topology of the original finite element mesh, but also because it does not impose restrictions with respect to the orientation of the crack planes. It is for these two reasons that the smeared concept quickly replaced the early discrete concepts and came into widespread use during the 1970s.

Bažant and Oh[11] introduce a model where a heterogeneous material such as concrete can be modeled as a band of densely distributed microcracks with a blunt front. When a heterogeneous material is approximated by an equivalent homogenous continuum (without couple stresses), as is standard for concrete structures, one must distinguish the continuum stresses and strains (macrostresses and microstrains) from the actual stress and strain in the microstructure, called the microstresses and microstrains. In the theory of the randomly inhomogeneous materials, the equivalent continuum stresses and strain are defined as the averages of the microstresses and microstrains over a certain representative volume. The cross section of this volume should be ideally taken to be much larger than the size of the inhomogeneities, and even for a crude modeling must be considered to

be at least several times their size, e.g., several times the maximum aggregate size in case of concrete.

Consequently, in the usual analysis, in which only the average elastic (or inelastic) material properties are considered and the geometry of the microstructure with the differences in the elastic constants between the aggregate and the cement paste is not taken into account, the distribution of stress and strain over distance less than several aggregate sizes has no physical meaning. Only the stress resultants and the accumulated strain over the cross section of the characteristic volume do. In the finite element context, this means, therefore, that it makes no sense to use finite elements smaller than several aggregates sizes. In case of fracture, this further means that if an equivalent homogenous continuum is assumed, it makes no sense to consider concentrations of stress (or of microcrack density) within volumes less than several aggregat sizes. A similar conclusion follows when we realize that the actual crack path in concrete is not smooth but highly tortuous. Since the crack tends to pass around the hard aggregate pieces and randomly sways to the side of a straight path by distances roughly equal to the aggregat size, again the actual stress (microstress) variation over such distances can be relevant for the macroscopic continuum model. According to the foregoing justification, one should not attempt to subdivide the width of the crack band front into several finite elements.

Various measurements are being made to observe the formation of microcracks at the fracture front[12,13]. From these observations, it seems that the larger microcracks that can be seen are not spread over a band of large width but are concentrated essentially on a line. However, the line along which the microcracks are scattered is not straight but is highly tortuous, deviating to each side of the straight line extension by a distance equal to about the aggregate size, as the crack is trying to pass around the harder aggregate pieces. In the equivalent, smoothed macroscopic continuum which is implied in structural analysis, the scatter in the locations of visible microcrakcs relative to a straight line is characterized by a microcrack better than by a straight row of microcracks.

At the same time, we should realize that the boundary of the fracture process zone should not be defined as the boundary of visible microcracks, but as

the boundary of the strain – softening region. Since the strain softening is caused not only by microcracking but also by any bond ruptures, the fracture process zone could be much wider (as well as longer) than the region of visible microcracks.

Equivalence of Smeared Crack and Cohesive Crack

For an elastic material which the stress drops suddenly to zero at the fracture front, it was found that a sharp inter-element crack and a smeared crack band give essentially the same results for the energy release rate and agree closely (within a few percent) with the exact elasticity solution, provided that the finite element is not larger than about $\frac{1}{15}$ of the cross section dimension (square meshes without any singularity elements were used). This is true regardless to the aggregate size[11].

The same equivalence of line cracks and crack bands may be expected when a gradual stress drop is considered. The reason for this equivalence is that the fracture propagation depends essentially on the flux of energy into the fracture process zone at the crack front, and this flux is a global characteristic of the entire structure.

The basic concept of crack band model, which was proposed in general terms in Bažant (1976) and was developed in full detail for sudden cracking in Bažant and Cedolin (1979, 1980, 1983) and Cedolin and Bažant (1980) and for gradual strain softening in Bažant (1982) and Bažant and Oh (1983a), is that the given constitutive relation with strain softening must be associated with a certain width of h_c of the crack band, which represent a reference width and is treated as a material property.

In Bažant approach, the width of the band cannot be less than a certain characteristic value h_c, therefore an expression will be obtained as:

$$h_c \varepsilon^f = w \qquad \text{(Eq. 2.1.1)}$$

where ε^f is the *inelastic fracturing* strain, graphically defined as shown in figure I.2 and w is the cohesive crack opening displacement. Thus, the stress – elongation curve for the band model and for the cohesive model will coincide if

one relate the softening of stress vs. fracturing strain $\phi(\varepsilon^f)$ to the softening curve of stress vs. crack opening of the cohesive crack :

$$\phi(\varepsilon^f) = f(w) = f(h_c \varepsilon^f) \quad or \quad f(w) = \phi\left(\frac{w}{h_c}\right) \qquad \text{(Eq. 2.1.2)}$$

where *f(w)* is the equation of the softening curve for the cohesive crack model. Therefore, there is a unique relationship between the crack band model and the cohesive crack model, at least for the simple elastic – softening case. The correspondence is illustrated in figure I.3 which shows the softening curve for cohesive crack (a) and the corresponding stress strain curve for the crack band (b). Also shown in the correspondence for the initial linear approximation to the curve, the horizontal intercept of which satisfies $\varepsilon_1 = \frac{w}{h_c}$. It follows that a linear approximation for the softening crack band will be a good approximation in the same circumstances as it was for the cohesive crack model.

Figure 2.1. 1.Correspondance between the softening curve of the cohesive crack model (a) and the stress – strain curve of the crack band model (b)

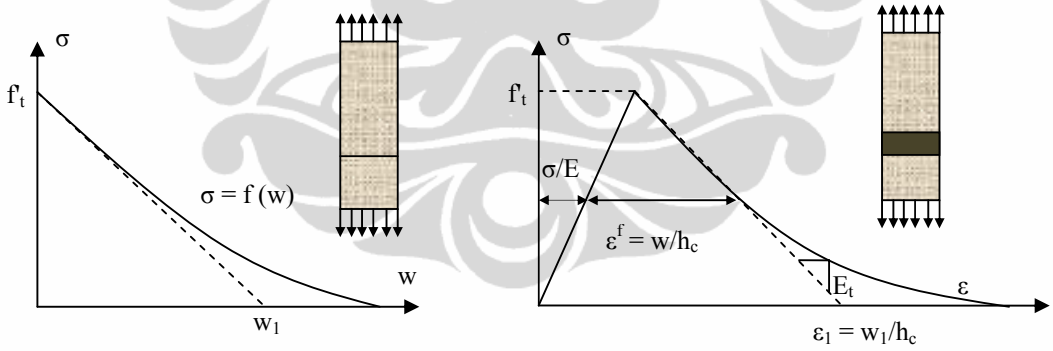

Therefore, the softening curves for cohesive crack can be directly implemented in the crack band model. The only difference between the result for cohesive crack model and crack band model is in the strain and displacement distribution. Figure 2.1.2 show the comparison of the axial displacement distribution. Obviously, the difference is nil for engineering purposes if $h_c \ll L$.

The correspondence is obviously maintained for the specific fracture energy G_f. It follows that the energy required to form a complete crack is

$$G_F = \frac{W_F}{A} = h_c \gamma_F \quad \text{(Eq. 2.1.3)}$$

where W_F is the total supply work, A is the area of the cross section of the bar. In terms of the properties of the crack band model, the characteristic size l_{ch} can be obtained as

$$l_{ch} = \frac{E G_F}{f_t'^2} = h_c \frac{E \gamma_F}{f_t'^2} \quad \text{(Eq. 2.1.4)}$$

A parameter of interest in numerical calculation using the crack band model is the softening modulus E_t for the linear approximation. It is shown that

$$2l_{ch} = h_c \left(1 - \frac{E}{E_t}\right) \quad \text{(Eq. 2.1.5)}$$

From here, we can derived the equation for the fracture energy as :

$$G_f - h_c \left(1 - \frac{E}{E_t}\right) \frac{f_t'^2}{2E} \quad \text{(Eq. 2.1.6)}$$

Figure 2.1. 2. Comparison of the distribution of axial displacement in a bar for the cohesive crack model (a, b) and crack band model (c, d)

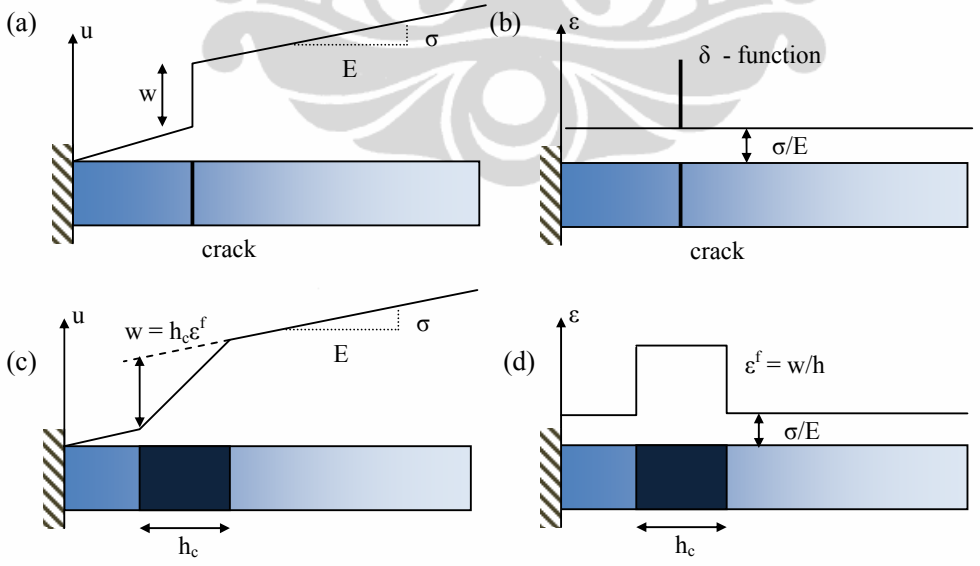

Crack Band Width

In a finite element formulation with free element size, the strain – softening curve must be adjusted according to the element size so that the calculation would yield macroscopically consistent result whatever the element size. This is close to saying that the crack band width h_c is arbitrary since it is replaced by the size of the element $h^{(e)}$ without a noticeable effect (as long as the element size is kept small). This means that h_c cannot be determined from fracture tests in which a single crack is formed[14].

The value of h_c, however, does have an effect in those situations where cracking does not localize but remains distributed over large zones. Thus the value of h_c can be identified only by comparing the results of fracture tests with the result of tests in which the cracking is forced to be distributed.

In a crude manner, the value of h_c can be approximately identified from fracture tests for specimens of various geometries, in which the cracking is localized to a different extent. This has been done in Bažant and Oh (1983a); with the conclusion that the crack band width $h_c = 3d_a$ where d_a is the maximum aggregate size, is approximately optimal. However, the optimum was weak, and crack band width anywhere between $2d_a$ and $5d_a$ would give almost equally good results.

Computational Notes

From this point of view, the crack band is more advantageous than the line crack model. When the crack extends through a certain node, the node must be split into two nodes, increasing the total number of nodes and changing the topological connectivity of the mesh. Unless all nodes are renumbered, the band structure of the structural stiffness matrix is destroyed. All this complicates programming.

With the crack band model, crack is modeled by changing the isotropic elastic moduli matrix into an orthotropic one, reducing the material stiffness in the direction normal to the cracks in the band. This is easily implemented in a finite element program, regardless of the direction of the crack with respect to the mesh lines[11].

However as this concept had been implemented in large finite element codes, it was discovered that the convergence properties are incorrect and the calculation results are unobjective as they significantly depend on the analyst's choice of the mesh (Bažant 1976, 1983; Bažant and Cedolin 1979, 1980, 1983; Bažant and Oh 1983a; Darwin 1985; Rots et al. 1985).

Figure 2.1. 3. Illustration of lack of mesh-objectivity in classical smeared crack models (adapted from ACI Committee 446 1992)

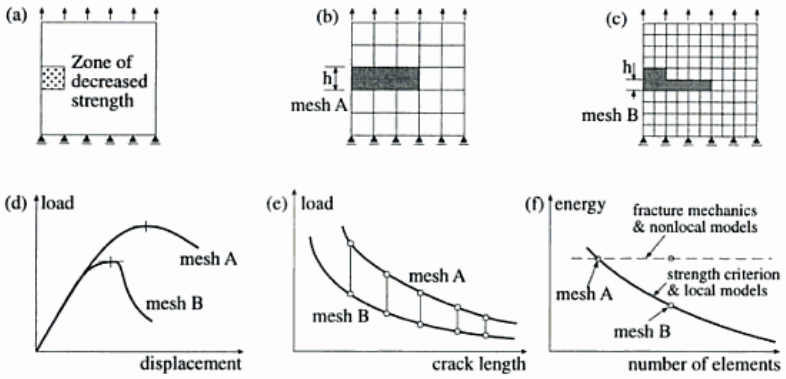

The problem, known as spurious mesh sensitivity, can be illustrated, for example, by the rectangular panel shown in figure 2.1.3, which is subjected to a uniform vertical displacement at the top boundary. A small region near the center of the left side is assumed to have a slightly smaller strength than the rest of the panel, and consequently a smeared crack starts growing from left to right. The solution is obtained by incremental loading with two finite element meshes of very different mesh sizes, as shown in the figure 2.1.3b,c. Stability check indicates that cracking must always localize in this problem into a band of single – element width at the cracking front. Typical numerical results for this as well as other similar problems are illustrated in figure 2.1.3d – f. in the load – deflection diagram (fig. 2.1.3d), one can see that the peak load as well as the post – peak softening strongly depends on the mesh size, the peak load being roughly proportional to $h^{-1/2}$ where h is the element size. Plotting the load vs. the length of the crack band, one again finds large differences (fig 2.1.3f) and converges to zero as $h \rightarrow 0$, which is, physically unacceptable.

Therefore, an approach is needed in order to overcome this this sensitivity of the numerical result. There are two main approaches are :

1. Adjustment of the softening law with respect to h_c so that the dissipated energy is independent of the size of the finite elements[11]
2. Application of a localization limiter, which leads to a size of the localization zone independent of the discretization.

2. 2. SIZE EFFECT

By general convention, the load capacity predicted by plastic limit analysis or any (deterministic) theory in which the material failure criterion is expressed in terms of stress or strain (or both) are said to exhibit no size effect, the size effect represents the deviation from such a prediction, i.e., the size effect on the structural strength is rate deviation, engendered by a change of structure size, of the actual load capacity of a structure from the load capacity predicted by plastic limit analysis[14].

The size effect is rigorously defined through a comparison of geometrically similar structures of different sizes [15]. It is conveniently characterized in terms of the nominal strength, σ_{Nu}, representing the value of the nominal stress, σ_N, at maximum load P_u. the nominal stress, which serves as load parameter, may, but need not, represent any actual stress in the structure and may be defined simply as

$$\sigma_N = \frac{P}{bD} \qquad \text{(Eq. 2.2.1)}$$

when the similarity is two-dimensional or as

$$\sigma_N = \frac{P}{bD^2} \qquad \text{(Eq. 2.2.2)}$$

when the similarity is three dimensional; b is the thickness of a two-dimensional structure, and D is the characteristic dimension of the structure, which may be chosen as any dimension, e.g., the depth of the beam, or the span, or half of the span, since only the relative values of σ_N matter. The nominal strength is then

$$\sigma_{Nu} = \frac{P}{bD} \text{ or } \frac{P}{bD^2} \qquad \text{(Eq. 2.2.3)}$$

According to the classical failure theories, such as the elastic analysis with allowable stress, plastic limit analysis, or any other theory that uses some type of strength limit or failure surface in terms of stress or strain, σ_{Nu} is constant, i.e., independent of the structural size, for any given geometry, notched or not. If we plot log σ_{Nu} vs. log D, we find that the failure states, according to the strength or yield criteria, to be always given by a horizontal line (figure I.1*)*. So the failures according to the strength or yield criteria exhibit no size effect.

By contrast, failures governed by linear elastic fractures mechanics exhibit a rather strong size effect, which is described by the inclined dashed line of slope -½. The reality for concrete structures is a transitional behavior illustrated by the solid curve. This curve approaches a horizontal line for the strength criterion if the structures are very small and inclined straight line of slope – ½ if the structure is very large.

2.2. 1. Transitional Size Effect for Different Scales

Below is a simple explanation of the deterministic size effect due to energy release[16]. Consider a rectangular panel shown in figure 2.2.1, which is initially under goes a uniform stress equal to the nominal stress σ_N. introduction of a crack of length a with a fracture process zone of a certain length and width h may be approximately imagined to relieve the stress and thus release the strain energy from the areas of the shaded triangles and the crak band shown in figure 1.4. the slope of the effective boundary of the stress relief zone, k, is a constant when the size is varied. We may assume that, for the range of interest, the length of the crack at maximum load is approximately proportional to the structure size D while the size h of the fracture process zone is essentially a constant, related to the inhomogeneity size in the material.

For very large structure sizes, the crack band width h becomes negligible compared to the structure's dimensions, and then the energy is getting released only from the shaded triangular zones (figure 1.4) whose area is proportional to D^2. This means that the energy released is proportional to

$$\frac{D^2 \sigma_N{}^2}{E} \qquad \text{(Eq. 2.2.4)}$$

where E is the Young Modulus. At the same time, the energy consumed is proportional to the area of the band of constant width h which in turn is proportional to D. So the energy consumed and dissipated by fracture is proportional to $G_f D$, where G_f is the fracture energy. Thus

$$\frac{D^2 \sigma_N{}^2}{E} \propto G_f D \qquad \text{(Eq. 2.2.5)}$$

Then it immediately follows that the size effect law for very large structures is

$$\sigma_N \propto D^{-1/2} \qquad \text{(Eq. 2.2.6)}$$

Figure 2.2. 1. Approximate zone of stress relief in small and large structures[7]

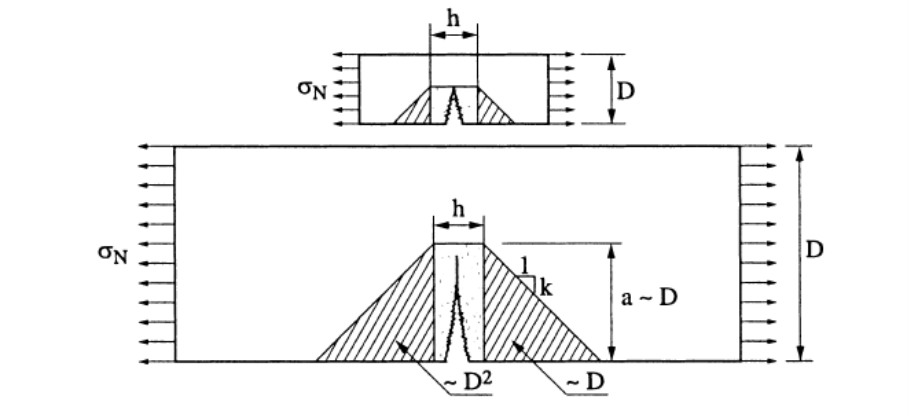

On the other hand, if the structure is very small, the triangular stress relief zones have a negligible area compared to the area of the crack band, which means that the energy release is proportional to

$$\frac{D \sigma_N{}^2}{E} \qquad \text{(Eq. 2.2.7)}$$

Therefore, the energy balance requires that

$$\frac{D\sigma_N^2}{E} \propto G_f D \qquad \text{(Eq. 2.2.8)}$$

from which it follows σ_N is constant. So, for very small structures, there is no size effect.

Figure 2.2. 2. Load – Deflection Curves for quassibrittle materials of different sizes[7]

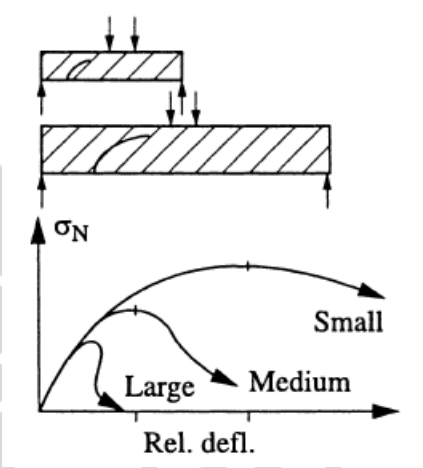

On the other hand, the curves of nominal strength versus the relative structure deflection have, for small and large structures, the shapes indicated in figure 2.2.2. Aside from the size effect on the maximum load, there is a size effect on the shape of the post – peak descending load – deflection curves. For small structures, the post – peak curves descend slowly while for larger structures, it descend steeper, and for sufficiently larger structures, it may even exhibit a snapback, which is a change of slope from negative to positive.

Therefore, it can be seen that small quasibrittle structures have a high ductility while large quasibrittle structures have a low ductility.

2.2. 2. Size Effect from Crack Band Theory

To illustrate the size effect resulting from the crack band theory, one can consider first a plain concrete center-cracked rectangular panel (figure 2.2.3) of thickness b, width $2d$, and a sufficiently large length $2L$[16]. The panel is loaded by vertical normal stresses σ at top and bottom. The crack band is horizontal, symmetrically located, and has length $2a$ and width $w_c = nd_a$.

The next step is to determine the value of σ which the crack band propagates. Before cracking, the strain energy density in the panel is uniform and equals to $\frac{\sigma^2}{2E}$. The formation of the crack band may be imagined, as an approximation, to relieve strain energy and stress from the stress relief area 1234561 in figure 2.2.3 (a), in which the stress diffusion line 25, 45, 16, 36 have a certain fixed slope k_1 (close to 1). Thus the total energy release from the panel is

$$W = W_1 + W_2 \qquad \text{(Eq. 2.2.9)}$$

in which :

$$W_1 = 2k_1 a^2 b \frac{\sigma^2}{2E} \text{ and } W_2 = 2nd_\alpha ab \frac{\sigma^2}{2E} \qquad \text{(Eq.2.2.10)}$$

Considering the top and bottom boundaries to be fixed during cracking, and therefore the contribution of the work of load σ applied at the boundaries is zero. So, the potential energy release rate of the panel is

$$\frac{\delta W}{\delta a} = 2(k_1 a + nd_\alpha)\frac{b\sigma^2}{2E} \qquad \text{(Eq.2.2.11)}$$

Due to the requirement of energy balance, $\frac{\delta W}{\delta a}$ must be equal to the energy consulted per unit crack band extension

$$\frac{\delta W}{\delta a} = G_f b \qquad \text{(Eq.2.2.12)}$$

Figure 2.2. 3. Examples of Crack Band Propagation[8]

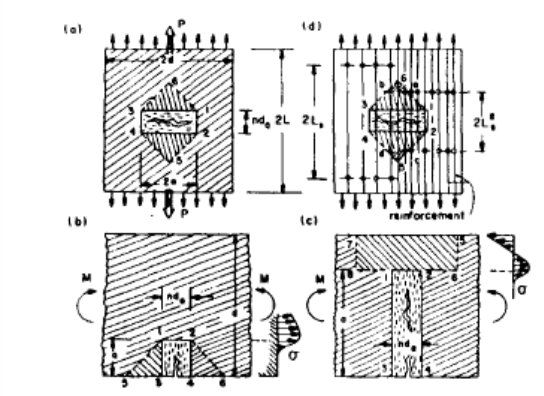

After substituting for G_f from equation 2.1.6, an equation from which is obtained as the following solution :

$$\sigma_N = B f_t^* \text{ where } \sigma_N = \sigma \qquad \text{(Eq.2.2.13)}$$

$$f_t^* = \frac{f_t}{\sqrt{1+\frac{\lambda}{\lambda_0}}} \qquad \text{(Eq.2.2.14)}$$

and

$$B = \sqrt{1+\frac{E}{-E_t}}\,;\ \lambda_0 = \frac{n}{2k_\perp}\frac{d}{a} \qquad \text{(Eq.2.2.15)}$$

in which $\lambda = \frac{d}{d_a}$ is relative to structure size; while B and λ_0 is constant when geometrically similar beams are considered. They are independent of size. Meanwhile, f_t* may be called as the *size reduced strength*. It is a characteristic of the entire structure, rather than a material.

Equation 2.2.14 can be similarly derived for various other situation, e.g., edge-cracked panels, crack band in infinite medium, etc. The solutions are approximate in the evaluation of energy release; however, the approximate nature of the solution causes uncertainty only in the constants k_1 and k_0, but not the form of equation 2.2.14.

CHAPTER 3
MODELLING TECHNIQUES

In this chapter, the damage model that the author will use for numerical analysis is to be described. Also, two approaches of numerical techniques in order to permit arbitrary mesh refinement and overcome the problem of mesh sensitivity of the numerical analyses will be discussed.

3. 1. MAZARS DAMAGE MODEL

The model of behavior of Mazars[17] is a simple model based on the damage mechanics[18], which makes it possible to describe the decrease of material under the effect of the microcracks propagation in concrete. It relies on a single internal scalar variable *D*, describing the damage isotropically, but still distinguishing the damage of traction and compression. Mazars damage model does not allow the phenomenon of reclosing of the cracks (restoration of rigidity). Moreover, it does not take a count of any plastic deformations or viscous effects that can be observed during the deformation of concrete.

3.1. 1. Description of the Model

Evolution of damage is considered isotropic and therefore the damage variable *D* is a scalar, which varies from 0 (without damage) until 1 (completely damaged). Stress is given by equation below :

$$\sigma = (1 - D)\,\mathbf{A}\,\varepsilon^{e} \qquad \text{(Eq. 3.1.1)}$$

where **A** is the matrices of hooke and ε^{e} is the elastic deformation.

The damage variable *D* is a combination of damage of traction D_t and damage of compression D_c :

$$D = \alpha_t^{\beta} D_t + \alpha_c^{\beta} D_c \qquad \text{(Eq. 3.1.2)}$$

The coefficient β is a material parameter, when it is higher than 1, it is possible to improve the result of shear. The damage is controlled by the equivalent strain ε_{eq} which allows one to describe the triaxial state from equivalence of an uniaxial state. As extensions are essential in the phenomenon of cracking of concrete, the equivalent strain introduced is determined from eigenvalues of positive strain tensor, such as :

$$\varepsilon_q = \sqrt{\langle \varepsilon_1 \rangle_+^2 + \langle \varepsilon_2 \rangle_+^2 + \langle \varepsilon_3 \rangle_+^2} \qquad \text{(Eq. 3.1.3)}$$

where ε_i is the principal deformation. In this equation, $\langle \varepsilon_i \rangle_+$ equals to ε_i when $\varepsilon_i \geq 0$ and equals to zero when $\varepsilon_i < 0$.

The damage variables of traction and compression is described below when $\varepsilon_{eq} \geq \varepsilon_{d0}$

$$D_t = 1 - \frac{\epsilon_{D0}(1 - A_t)}{\epsilon_{eq}} - A_t \exp[-B_t(\tilde{\epsilon} - \epsilon_{D0})] \qquad \text{(Eq. 3.1.4)}$$

$$D_c = 1 - \frac{\epsilon_{D0}(1 - A_c)}{\epsilon_{eq}} - A_c \exp[-B_c(\tilde{\epsilon} - \epsilon_{D0})] \qquad \text{(Eq. 3.1.5)}$$

where A_t, A_c, B_t, B_c are the parameters to be found.

The determination of α_t and α_c in equation 3.1.2 is done by using the deformations ε_{ti} and ε_{ci} due to the positive and negative principal stresses respectively as shown below :

$$\alpha_t = \sum_{i=1}^{3} H_i \frac{\varepsilon_{ti}(\varepsilon_{ti} + \varepsilon_{ci})}{\tilde{\varepsilon}^2} \qquad \text{(Eq. 3.1.6)}$$

$$\alpha_c = \sum_{i=1}^{3} H_i \frac{\varepsilon_{ci}(\varepsilon_{ti} + \varepsilon_{ci})}{\tilde{\varepsilon}^2} \qquad \text{(Eq. 3.1.7)}$$

H_i equals to 1 if $\varepsilon_i = \varepsilon_{ti} + \varepsilon_{ci} \geq 0$, or else H_i equals 0. From the equation 3.1.6 and 3.1.7, it can be verified that for uniaxial loading of tension, $\alpha_t = 1$, $\alpha_c = 0$, $D = D_t$ and vice versa for compression. The constitutive model is finally described as :

$$\sigma = (1 - D)\mathbf{A} : \varepsilon \qquad \text{(Eq. 3.1.8)}$$

with σ and ε as the second order tensor of stress and deformation and $\mathbf{A}$ is the fourth order of modulus elasticity.

3.1. 2. Identification of parameters

Besides the thermo – elastic parameters such as E, υ, α, there are six parameters to be defined in Mazars damage model, which are A_t, A_c, B_t, B_c, ε_{d0}, β.

Figure 3.1. 1. Influence of A Parameters (a) and B Parameters (b)

(a)

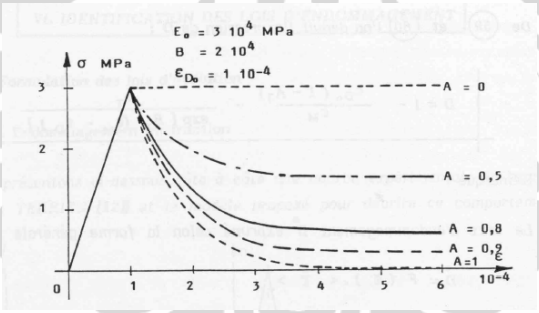

(b)

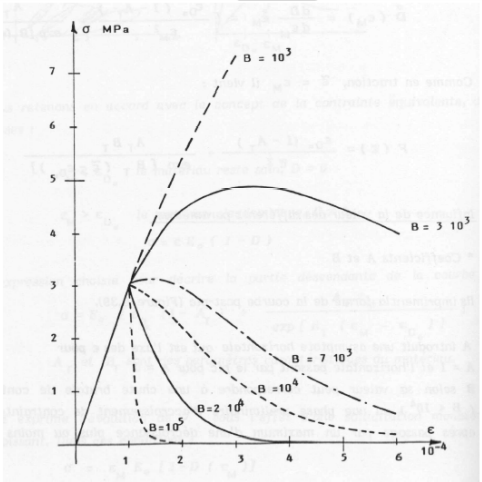

a. ε_{d0} is the damage threshold. This value influences the stress at peak as well as the curve of post peak. The stress drop will be less brittle if the value of ε_{d0} is small. Normally, ε_{d0} is taken as 0,5 until 1,5 10^{-4}.
b. Coefficients of A influence the part of post-peak curve. This coefficient gives the horizontal asymptote of ε axis when A equals to 1 and a horizontal line passing the peak if A is taken as 0.
c. Coefficients of B also influence the part of post – peak curve. Based on its value, B may influence a stress drop if the value is too high (B > 10000). Normally, B_c is taken between 1000 – 2000 and B_t is taken between 10000 – 100000.
d. β is a corrective factor which makes it possible to improve the result in shearing compared to the initial version of the model (which corresponds to β =1). Normally, the value used is 1.06.

3. 2. FICTITIOUS CRACK MODEL BY HILLERBORG

Hillerborg et al[19]. first introduce a fictitious crack model for fracture of concrete. Fictitious crack approach basically assumes that energy to create the new surfaces is small compared to one required to separate them. As a result, the energy dissipation for crack propagation can be characterized by the cohesive stress separation :

$$G_q = \int_o^{w_t} \sigma(w)dw \qquad \text{(Eq. 3.2.1)}$$

This equation is valid for structures with a unit constant thickness.

Figure 3.2. 1. Principle for fictitious crack model by Hillerborg : (a) complete stress-elongation curve

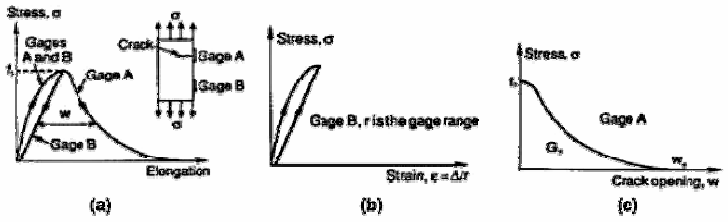

In the Hillerborg approach, typical stress – elongation curve for concrete plate subjected to uniaxial tension is shown in figure 3.3.1 (a). The elongation of the plate is measured by two displacement gages, gage A and gage B, respectively. Gage A is assumed to measure the elongation including the cracked section, while gage B is to measure the elongation outside the cracked section. It is assumed that strain localization appears only after the maximum load is reached. As a result, the elongation at the location of gage A continuously increasing whereas the location of gage B is unloading due to the strain localization. The area under the entire softening stress-elongation curve $\sigma(w)$ is given by

$$G_F = \int_0^{w_c} \sigma(w)dw \qquad \text{(Eq. 3.2.2)}$$

where w_c is the critical crack separation displacement when the softening stress is equal to zero.

In the fictitious crack model, the softening – separation curve $\sigma(w)$ is assumed to be a material property that is independent of structural geometry and size. This model requires three material parameters : the value of f_t, G_f and the shape of the $\sigma(w)$ curve (the softening behaviour). When the shape of the $\sigma(w)$ curve is determined, the material fracture property is known by the values of f_t and G_f. In this case, it is also suitable to combine f_t and G_f into a characteristic length

$$l_{ch} = \frac{EG_F}{f_t^2} \qquad \text{(Eq. 3.2.3)}$$

The Hillerborg model underlines the general principles for crack analysis in concrete. First, it illustrates the fundamental importance of the tension – softening cracking. Second, it shows that after cracking, the general deformation of the cracked body is composed by two parts: the deformation of the elastic part and the crack – opening width of the crack. Third, the elastic body outside the cracking is subjected to the stress transferred through the fictitious crack, and therefore its deformation is also a function of $\sigma(w)$.

3. 3. LA BORDERIE APPROACH

La Borderie[20] introduced a method to extract a crack opening from a continuum damage finite element computation. With the basic idea of the Crack Band Theory, as been discussed in the previous chapter, instead of treating cracks as lines, Bažant and Oh[21] consider the fracture zone to have a certain width h_c over which micro-cracks are uniformly distributed. The bandwidth h_c is regarded as a material parameter. It is required in order to avoid spurious mesh sensitivity and achieve objectivity. The energy dissipation due to fracture per unit length (or unit width) is, therefore, a constant. The fracture energy is given by

$$G_f = \int_0^\infty \sigma \, d\delta \qquad \text{(Eq. 3.3.1)}$$

where δ is the crack opening displacement.

According to this theory, the material behavior in the fracture process zone is characterized in a smeared manner through a strain-softening constitutive relation. Therefore the crack opening displacement is taken as the fracture strain accumulated over the width h_c or the finite element.

$$\delta = \varepsilon^{uco} h \qquad \text{(Eq. 3.3.2)}$$

where we consider ε^{uco} as the Unitary Crack Opening strain variable (fracture strain)[22].

The total strain in the fracture zone consists of an elastic portion and a fracture portion. Hence, the fracture energy per unit width is calculated as the area under the complete stress-strain diagram :

$$G_f = h \int_0^\infty \sigma \, d\varepsilon^{uco} = h \int_0^\infty \sigma \, d\varepsilon \qquad \text{(Eq. 3.3.3)}$$

The total strain in the fracture zone consists of an elastic portion and a fracture portion. Hence, the fracture energy per unit width is calculated as the area under the complete stress-strain diagram :

$$G_f = h\int_0^{\infty} \sigma \, d\varepsilon^{uco} = h\int_0^{\infty} \sigma \, d\varepsilon \qquad \text{(Eq. 3.3.4)}$$

If we consider the damage model presented above, the constitutive law is given by

$$\sigma_{ij} = (1 - d)C_{ijkl}\varepsilon_{kl} \qquad \text{(Eq. 3.3.5)}$$

Using the damage evolution law, the fracture energy is the area under a uniaxial tensile strain-stress diagram. Therefore, we obtain:

$$G_f = h\int_0^{\infty} ((1 - d)\, E\varepsilon)\, d\varepsilon \qquad \text{(Eq. 3.3.6)}$$

$$G_f = h\int_0^{\varepsilon_{d0}} E\varepsilon \, d\varepsilon + \int_{\varepsilon_{d0}}^{\infty} \frac{\varepsilon_{d0}}{\varepsilon} \exp[B\,(\varepsilon_{d0} - \varepsilon)]\; E\varepsilon \, d\varepsilon \qquad \text{(Eq. 3.3.7)}$$

The first part of the fracture energy corresponds to the elastic contribution where the damage has not yet occurred, thus $d = 1$.

$$\frac{G_f}{h} = \int_0^{\varepsilon_{d0}} E\varepsilon \, d\varepsilon + \int_{\varepsilon_{d0}}^{\infty} \frac{\varepsilon_{d0}}{\varepsilon} \exp[B\,(\varepsilon_{d0} - \varepsilon)]\; E\varepsilon \, d\varepsilon \qquad \text{(Eq. 3.3.8)}$$

The integration of the first part :

$$\frac{G_f}{h} = \frac{1}{2}E\varepsilon^2 \Big|_0^{\varepsilon_{d0}} = \frac{E[(\varepsilon_{d0})^2]}{2} \qquad \text{(Eq. 3.3.9)}$$

The integration of the second part :

$$\int_{\varepsilon_{d0}}^{\infty} \frac{\varepsilon_{d0}}{\varepsilon} e^{[B\,(\varepsilon_{d0} - \varepsilon)]}\; E\varepsilon \, d\varepsilon = E\varepsilon_{d0} e^{B_t\varepsilon_{d0}} \int_{\varepsilon_{d0}}^{\infty} \frac{1}{e^{B_t\varepsilon}} \, d\varepsilon$$

$$= E\varepsilon_{d0}e^{B_t\varepsilon_{d0}}\left(\lim_{\varepsilon\to\infty} -\frac{e^{-B_t\varepsilon}}{B_t} + \frac{e^{-B_t\varepsilon_{d0}}}{B_t}\right)$$

$$= \frac{E\varepsilon_{d0}}{B} \qquad \text{(Eq.3.3.10)}$$

Therefore, after the integration, the equation will be

$$\frac{G_f}{h} = \frac{f_t\varepsilon_{d0}}{3} + \frac{f_t}{B} \qquad \text{(Eq.3.3.11)}$$

with f_t the tensile strength and E the Young Modulus ($f_t = E \times \varepsilon_{d0}$). This leads to an independent-discretization energy release upon crack propagation. Initiation and propagation of cracks is governed by the material tensile stress and the fracture energy.

While the crack opening displacement is given by equation 3.3.2, the Unitary Crack Opening strain variable is computed using the following procedure :

The total strain in the fracture element is written as

$$\varepsilon_{ij} = \varepsilon_{ij}^{e} + \varepsilon_{ij}^{uco} \qquad \text{(Eq.3.3.11)}$$

The total strain is composed by an elastic part ε^{e} and a cracking part represented by the unitary crack opening strain variable ε^{uco}. Multiplying 3.3.11 by the elastic stiffness tensor C_{ijkl}, the equation will be

$$\bar{\sigma}_{ij} = C_{ijkl}\varepsilon_{kl} = C_{ijkl}\varepsilon_{kl}^{e} + C_{ijkl}\varepsilon_{kl}^{uco} = \sigma_{ij} + \sigma_{ij}^{in} \qquad \text{(Eq.3.3.12)}$$

So, the tensor of the crack opening will be

$$\varepsilon_{kl}^{uco} = C_{ijkl}^{-1}\sigma_{ij}^{in} \qquad \text{(Eq.3.3.13)}$$

From the finite element method, the nominal stress will be obtained. The inelastic stress tensor is given by

$$\sigma_{ij}^{in} - \sigma_{ij} - \bar{\sigma}_{ij} \qquad \text{(Eq.3.3.14)}$$

Equation 3.3.13 gives the unitary crack opening tensor. The normal crack opening displacement value is given by

$$\delta_n = n_i \delta_{ij} n_j = n_i h \varepsilon_{kl}^{ucr} n_j \qquad \text{(Eq.3.3.15)}$$

where *n* is the unit vector normal to the crack.

For the one – dimensional test :

$$\delta_n = h \varepsilon_{nn}^{ucr} \qquad \text{(Eq.3.3.16)}$$

3.3. 1. of Fracture Energy using Mazars Damage Model

Replacing the damage law used in equation 3.3.6 by the Mazars damage model in equation 3.1.2 for a problem of uniaxial tension, an equation can be derived. When material has not yet been damaged, *d* equals to zero and ε varies between 0 - ε_{D0}. Therefore, the equation will be:

$$G_f = h \int_0^{\varepsilon_{D0}} ((1 - 0) E\varepsilon)\, d\varepsilon + \int_{\varepsilon_{D0}}^{\infty} ((1 - d) E\varepsilon)\, d\varepsilon$$

$$G_f = h \int_0^{\varepsilon_{D0}} (E\varepsilon)\, d\varepsilon + \int_{\varepsilon_{D0}}^{\infty} ((1 - d) E\varepsilon)\, d\varepsilon \qquad \text{(Eq. 3.3.17)}$$

In the first part of equation 3.3.17

$$\frac{G_f}{h} = \frac{1}{2} E\varepsilon^2 \Big|_0^{\varepsilon_{d0}} = \frac{E[(\varepsilon]_{do}^2)}{2} \qquad \text{(Eq. 3.3.18)}$$

In the second part, where damaged already occurred :

$$G_f = h \int_{\varepsilon_{D0}}^{\infty} \left(\frac{\varepsilon_{D0}(1 - A_t)}{\varepsilon_{eq}} + A_t \exp[-B_t(\varepsilon - \varepsilon_{D0})] \right) E\varepsilon \, d\varepsilon \quad \text{(Eq. 3.3.19)}$$

$$\frac{G_f}{h} = \int_{\varepsilon_{D0}}^{\infty} \frac{\varepsilon_{D0}(1 - A_t)}{\varepsilon_{eq}} E\varepsilon \, d\varepsilon + \int_{\varepsilon_{D0}}^{\infty} A_t \exp[-B_t(\bar{\varepsilon} - \varepsilon_{D0})] \, E\varepsilon \, d\varepsilon \quad \text{(Eq. 3.3.20)}$$

The integration of the first part of equation 3.3.20

$$\int_{\varepsilon_{D0}}^{\infty} E\varepsilon \frac{\varepsilon_{D0}(1 - A_t)}{\varepsilon_{eq}} d\varepsilon = E\varepsilon_{D0}(1 - A_t) \left\{ \int_{\varepsilon_{D0}}^{\infty} \frac{\varepsilon}{\varepsilon_{eq}} d\varepsilon \right\} \quad \text{(Eq. 3.3.21)}$$

For a uniaxial load, ε_{eq} corresponds only on the x direction, therefore ε_{eq} equals to ε_{xx} which can simply equals toε.

$$= E\varepsilon_{D0}(1 - A_t) \left\{ \int_{\varepsilon_{D0}}^{\infty} 1 \, d\varepsilon \right\} \quad \text{(Eq. 3.3.22)}$$

For the case of concrete under uniaxial tension consider the material will always fail. For such conditions, the model parameter for A_t is 1.

$$= E\varepsilon_{D0}(1 - A_t) \left\{ \lim_{\varepsilon \to \infty} (\varepsilon - \varepsilon_{D0}) \right\} = 0 \quad \text{(Eq. 3.3.23)}$$

The integration of the second part of equation 3.3.20 is

$$\int_{\varepsilon_{D0}}^{\infty} A_t e^{\left[-B_t(\bar{\varepsilon} - \varepsilon_{D0})\right]} E\varepsilon \, d\varepsilon = A_t E \int_{\varepsilon_{D0}}^{\infty} \varepsilon \, e^{\left[-B_t(\bar{\varepsilon} - \varepsilon_{D0})\right]} d\varepsilon \quad \text{(Eq. 3.3.24)}$$

For a uniaxial load, $\bar{\varepsilon}$ corresponds only on the x direction, therefore $\bar{\varepsilon}$ equals to ε_{xx} which can simply equals toε

$$= A_t\, E\, e^{B_t \varepsilon_{D0}} \left\{ \int_{\varepsilon_{D0}}^{\infty} \varepsilon \frac{1}{e^{B_t \varepsilon}} d\varepsilon \right\} = A_t E \ \frac{B_t \varepsilon_{D0} + 1}{{B_t}^2} \qquad \text{(Eq. 3.3.25)}$$

Therefore, after the integration, an equation will be obtained

$$\frac{G_f}{h} = \frac{E\,[(\varepsilon]_{do}^2)}{2} + A_t E \ \frac{B_t \varepsilon_{D0} + 1}{{B_t}^2} \qquad \text{(Eq. 3.3.26)}$$

CHAPTER 4
NUMERICAL ANALYSIS

The numerical studies have used the CAST3M code for the calculation. Cast3M is a computer code for the analysis of structures by the finite element method (FEM). This code was developed by the Department of Mechanics and Technology (DMT) of the French Atomic Energy Commission (CEA). The general analysis carried out using the finite element method can be d4ided into three phases.

The first phase is the mathematical model definition. In this phase, geometrical discretizations are defined. The definition of the data describing the model, the type of analysis (strains or stresses plane, axisymetry, etc.), the type of element (beams, hulls, etc.), properties of material, meshes and the boundary conditions. The next phase is the discrete problem solving, where the calculation of the stiffness and the mass matrix is done. In this phase also, external loadings and the boundary conditions are applied. On the last phase, the result and post – processing are done. The result can be either local quantities (displacements, contraintes, strains) or global ones (maximum strain).

4. 1. ONE DIMENSION UNIAXIAL

4.1. 1. Model Definition

In the first section of the numerical analysis, a simple one dimension concrete bar is modeled as shown in figure 4.1.1. The size characteristic for the model are :

- Length $L = 1m$
- Height $b = 0.1m$

where the thickness of the beam is not being modeled and therefore, on the numerical modeling, it will be considered in a default criteria that the code has given.

Figure 4.1. 1. Model of the concrete bar

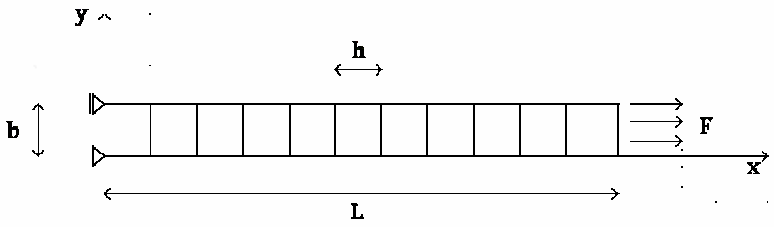

Meanwhile, the material parameters are

- Fracture Energy G_f= 100 *N/m*
- Young Modulus $E = 30 \times 10^9$ N/m^2
- Tensile strength $f_t = 3 \times 10^6$ N/m^2 while in the weak area, $f_t = 1 \times 10^6$ N/m^2
- Damage threshold $\varepsilon_{DO} = 10^{-4}$, while in the weak area, $\varepsilon_{DO} = 3.33 \times 10^{-5}$
- Poisson ratio is considered as 0 since the displacement of the bar is desired strictly on the x - direction

The bar is restrained on the left hand side on the horizontal (x) and vertical (y) direction. The right hand side of the bar is considered free, where the increment uniaxial load is imposed. In the middle of the bar (area of h shown in figure 4.1.1) weakness is adjusted, by reducing the value of tensile strength f_t. As the beam is imposed by the load, a tensile fracture zone starts developing as soon as the strain corresponding to the tensile strength f_t is exceeded. Therefore, crack propagation will be forced in the h area. Calculation will be made with four different numbers of elements m, i.e. m = 11, 21, 31, and 61. Computation is driven in plane stress, and the non-linier calculation is done by using an arc length method thus it will be possible to obtain better result of curve, since there is a possibility in reproducing curves with snapback.

4.1. 2. Local Calculation

The analysis begins with a simple local calculation, where Mazars damage law is simply implemented. The parameters of Mazars damage law are

Table 4.1. 1. Model parameters for local calculation

A_t	B_t	A_c	B_c	β
1	11000	1.2	30×10^3	1.06

The global result of force – displacement curve obtained for the four types of mesh refinement (figure 4.1.1) shows that obviously there is a mesh independency if we change the size of the elements. For each type of beam, the peak load does not change with the number of elements; however the brittle behavior does as the mesh is being refined. From the local behavior point of view, as shown in figure 4.1.2, mesh independency also occurs.

Figure 4.1. 2. Force – Displacement curve of local calculation

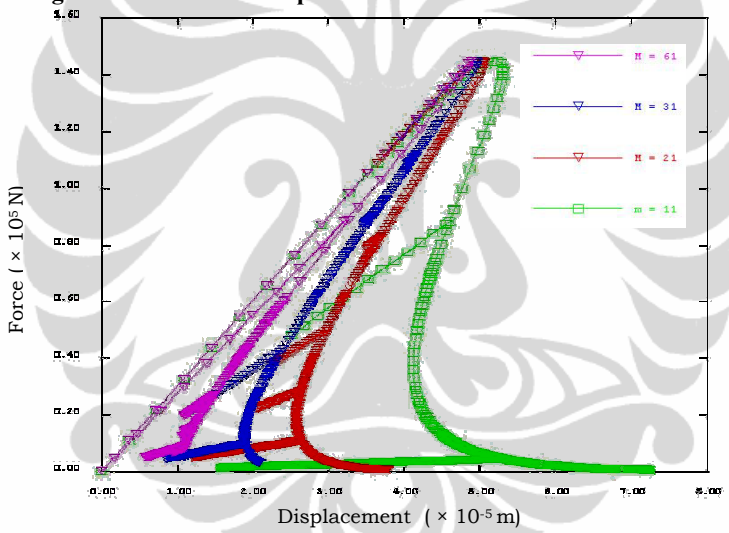

Figure 4.1. 3. Damage field for each different mesh refinement

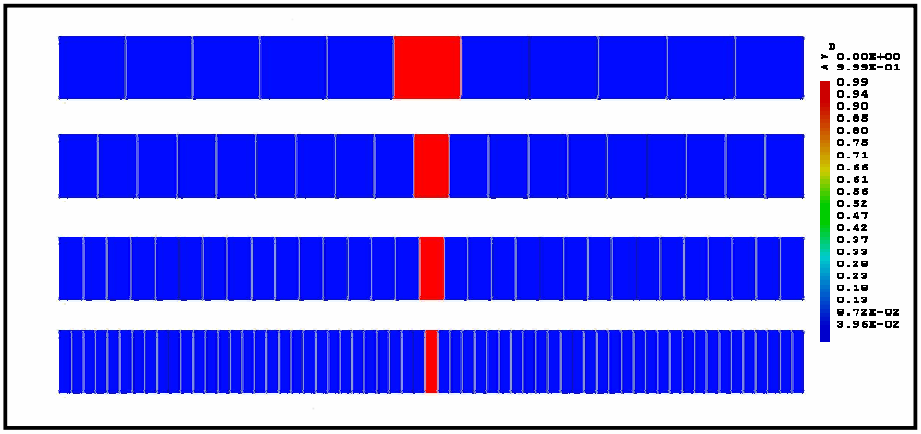

Hillerborg Approach Using Mazars Damage Law

In order to deal with the problem of mesh independency, one approach which is considered to be able to manage this problem is the Hillerborg approach. This model requires three material parameters: G_f, f_t, and the shape of the $\sigma(w)$ curve (the softening behaviour) that are considered as the material parameter independent of structural geometry and size. Thus there will be an adjustment with repect to h, as h is treated as a material property and is independent of the size of finite element. Implementing the Hillerborg approach in the Mazars damage law as mentioned in Equation 3.3.26, one may obtain the Mazars model parameters such as B_t and A_t, as these parameters are ones which give influence to the shape of the $\sigma(w)$ curve.

However, note that the tension parameters (B_t) in Mazar damage model give influences in the value of the peak load. Below, several stress – strain curves are presented to show the influence of these tension parameters. Therefore, it will be unobjective if the regularization of fracture energy depends on the B_t parameters

Other Mazars damage law parameter that can be used in order to regulate the G_f is the A_t parameter. A_t parameter does not influence the peak load of the $\sigma(w)$ curve. Below the values of A_t is presented for each type of element.

Figure 4.1. 4. Influence of B_t in the Stress – strain curve

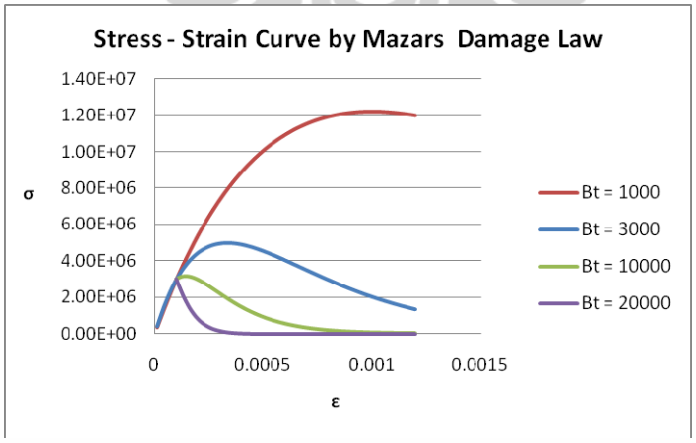

It can be seen that the values obtained for A_t are not relevant (except the value for m = 11 for $f_t = 3MPa$), since A_t is a parameter that ranges from 0 to 1. Therefore, Hillerborg approach is not suitable to be implemented in Mazars damage law.

Table 4.1. 2. Value of A_t for each number of elements

		f_t = 3 MPa		
	m = 11	m = 21	m = 31	m = 61
h	$\frac{1}{11}$	$\frac{1}{21}$	$\frac{1}{31}$	$\frac{1}{61}$
A_t	0.333	-0.273	-0.879	-2.670
		f_t = 1 MPa		
At	-0.304	-0.892	-1.481	-3.245

Hillerborg Approach with Modified Law by La Borderie

In this section, Hillerborg approach is done by using the evolution damage law conducted by La Borderie as mentioned in Equation 3.3.11. Table 4.1.3 gives the values of B_t for each type of h.

Table 4.1. 3. Value of B_t for each number of elements

		f_t = 3 MPa		
	m = 21	m = 31	m = 61	m = 11
h	$\frac{1}{11}$	$\frac{1}{21}$	$\frac{1}{31}$	$\frac{1}{61}$
B_t	3157,89	1538,46	1016,95	504,20
		f_t = 1 MPa		
B_t	922,12	479,51	323,	164,22

Global Result

After the values of B_t is obtained, they are implemented in the numerical calculation. Figure 4.1.4 shows the Force – Displacement curves, where the global result for each type of element is the same. Figure 4.1.5 shows the stress – Crack opening displacement (COD) graph. It can be seen that the mesh refinement does

not affect the curve. The fracture energy is represented by the area under the curve, and it is equal to the fracture energy used for simulation. Local Result

As shown in figure 4.1.4 and figure 4.1.5, the Hillerborg approach using evolution damage law is capable in giving the same global result for each different type of meshes. Meanwhile, as shown in figure 4.1.6a - d, the approach does not seem to be able to reproduce the same local behavior where the damage occurred seems to behave according to the mesh refinement. Therefore, another method is needed in order to simulate the local behavior independent form mesh refinements.

Figure 4.1. 5. Force – Displacement Graph by Hillerborg approach using evolution damage law

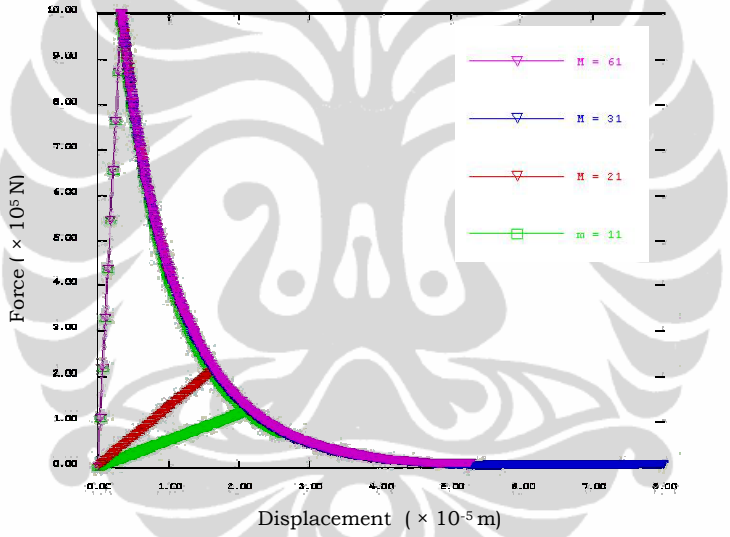

Figure 4.1. 6. Stress – COD Graph by Hillerborg Approach using Evolution Damage Law

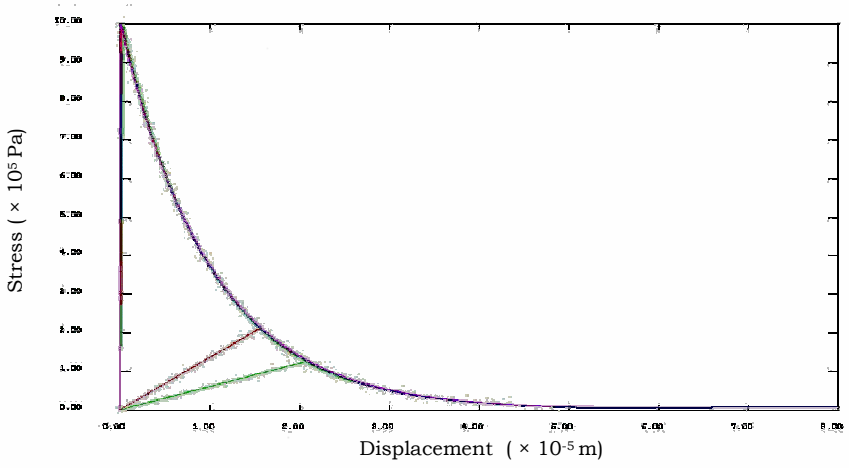

Figure 4.1. 7. Damage field for each mesh refinement, (a) 11, (b) 21, (c) 31, (d) 61

(a)

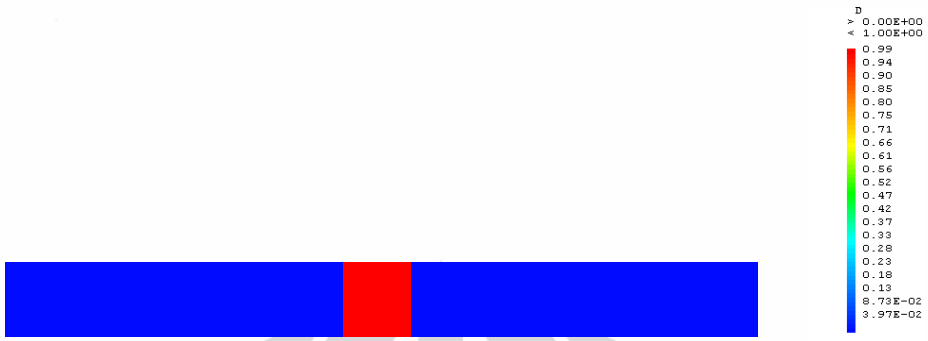

(b)

(c)

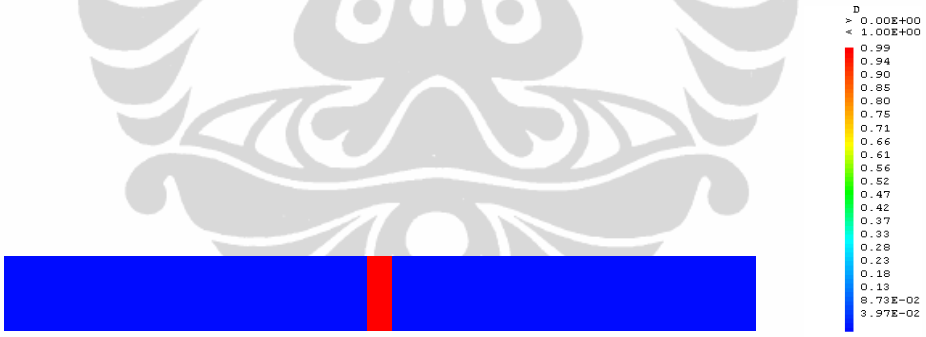

(d)

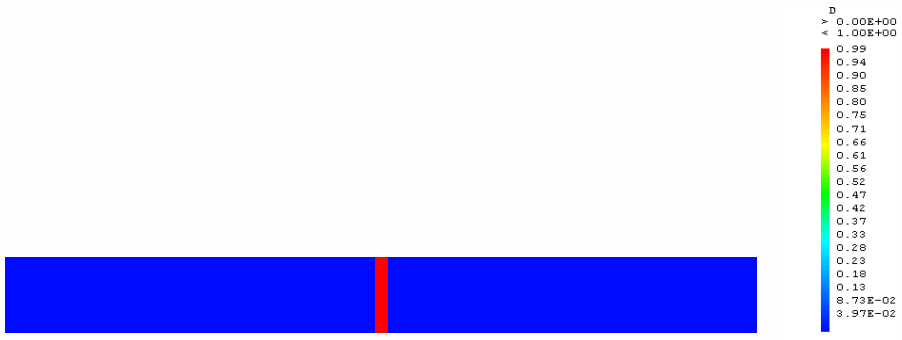

Figure 4.1. 8. Displacement field at final state for each mesh refinement, (a) 11, (b) 21, (c) 31

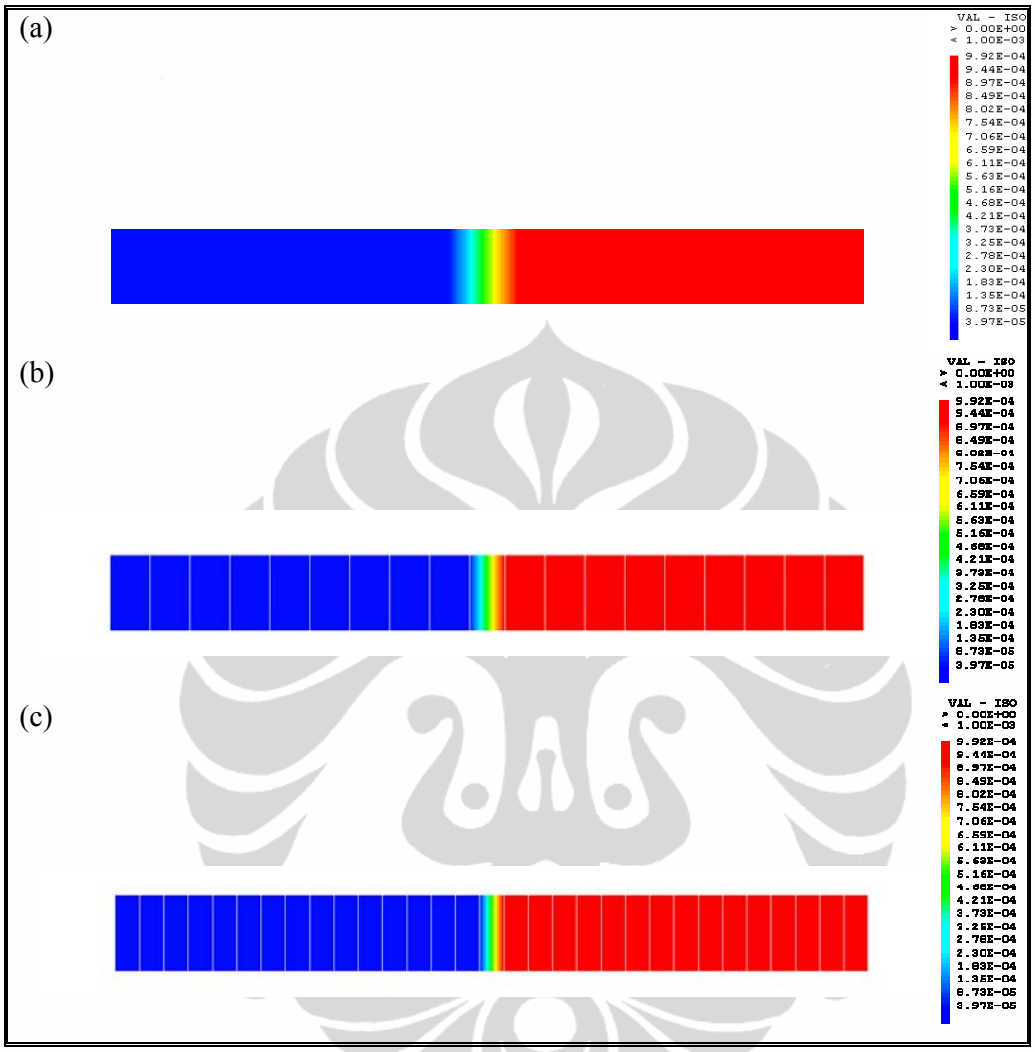

Crack Opening using Sum of Displacement and La Borderie Method

The crack opening can be calculated using two approaches; the sum of displacement and the crack opening displacement using La Borderie Method. The first approach is a classic method to obtain the crack opening by extracting the values from displacement tables; meanwhile the latter is an approach where another table is created to reproduce such values of crack opening. However, this approach may be conducted only the calculation is done by PASAPAS procedure.

Figure 4.1.7 and figure 4.1.8 compares the results of these two methods. Table 4.1.4 shows a comparison between the results of these two methods. It can

be seen that there is a difference in the value of each method, where the largest difference occurred in m = 21.

Figure 4.1. 9. COD field at final state for each mesh refinement, (a) 11, (b) 21, (c) 31

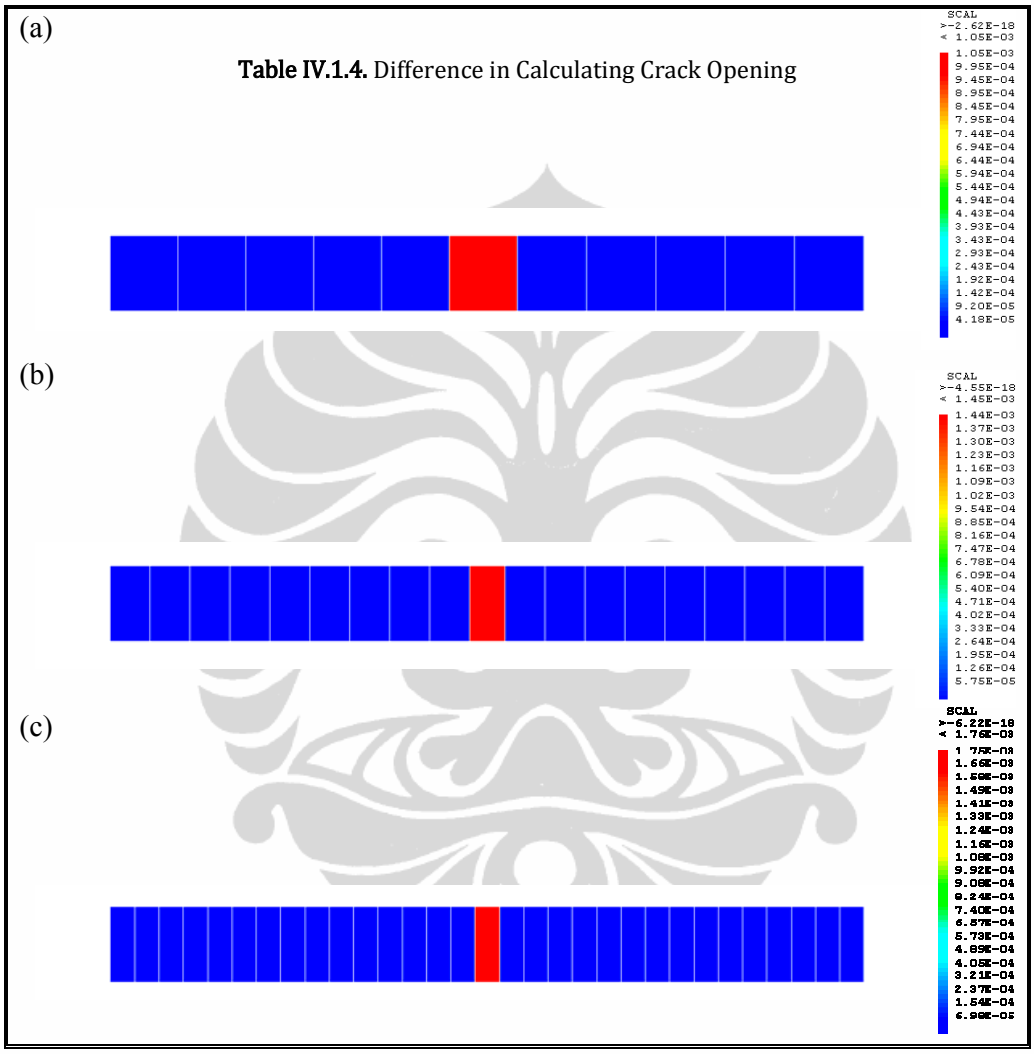

Table IV.1.4. Difference in Calculating Crack Opening

Table 4.1. 4. Difference in calculating crack opening

	m = 11	m = 21	m = 31
Sum of Displacement (m)	0,0009523	0,001049	0.,001549
La Borderie Method (mm)	0.00105	0.00144	0.0018
Difference (%)	9,35	27,15	11,48

4.1. 3. Non Local Calculation

Another approach which may overcome the problem of mesh sensitivity is the non – local approach. This approach uses a localization limiter which forces a specific size of an inelastic strain region which is independent of the mesh refinement.

However, a hindrance is found in modeling the non local calculation using CAST3M. It is figured that CAST3M is not able to connect two different types of material properties as shown in figure 4.1.10. This incapability leads to a situation where the size of localization is independent with the size of the element. Thus a localization limiter is not able to be implemented in CAST3M.

Figure 4.1. 10. CAST3M hindrance in lon local model

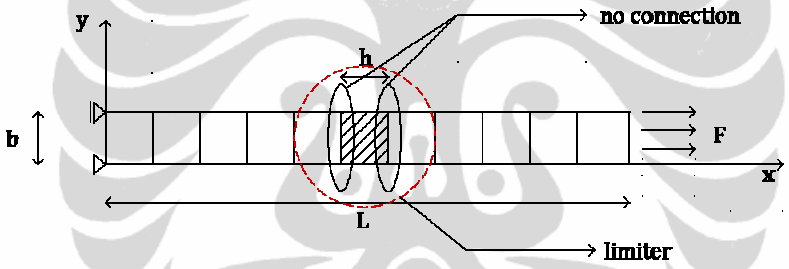

4.1. 4. Random Distributed Property Method

Since there is an obstacle in modeling a non – local damage model, another method is thus applied which uses the spatial variability of concrete properties and thus creates a randomly property field. This random Property method also overcomes the complicated condition of predicting the crack position and number.

In the random method, no such weak area h_c is defined so that the crack will not be forced in a specific area. Instead, the crack will be distributed along the beam. Computation is driven in plane stress. Standard model parameters have been chosen for the simulation. Damage model used in this calculation is the non – local Mazars Damage Law, with parameter used is given in table 4.1.1. Localization limiters used is 0,3.

Figure 4.1.11 shows the load – displacement curves for each types of mesh refinement. The result shows that in any type of mesh refinements, it gives almost the same value of peak load and almost the same shape of the curve._Meanwhile for the local result, which is represented by the damage field in figure 4.1.12, it satisfies the independency of mesh refinement. Damage occurs in such an area where it has been specified by the localization limiters.

Figure 4.1. 11. Force – Displacement graph using random distributed property

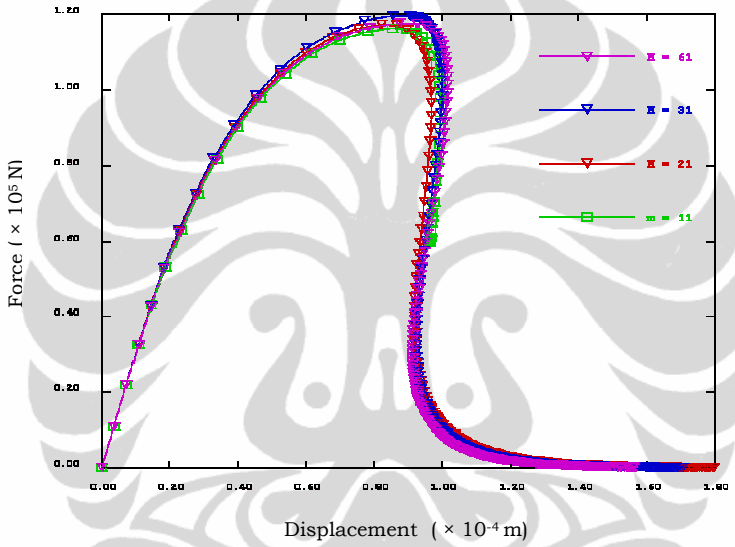

Figure 4.1. 12. Damage field by random distributed property method, for m = 11 (a), m = 21 (b), m = 31 (c), m = 61 (d)

(a)

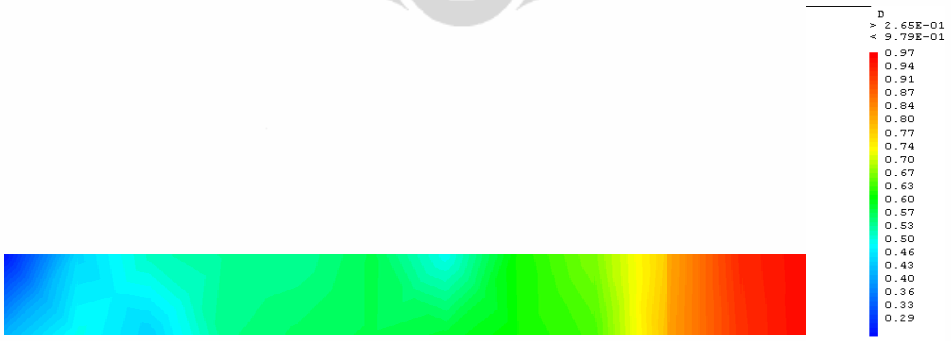

(b)

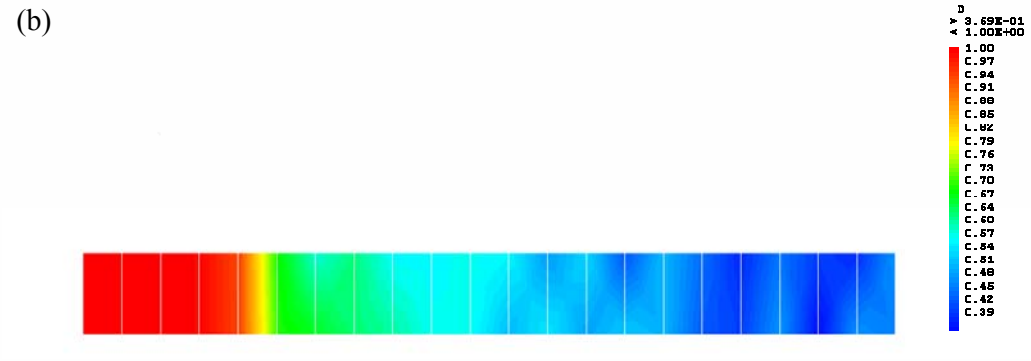

(c)

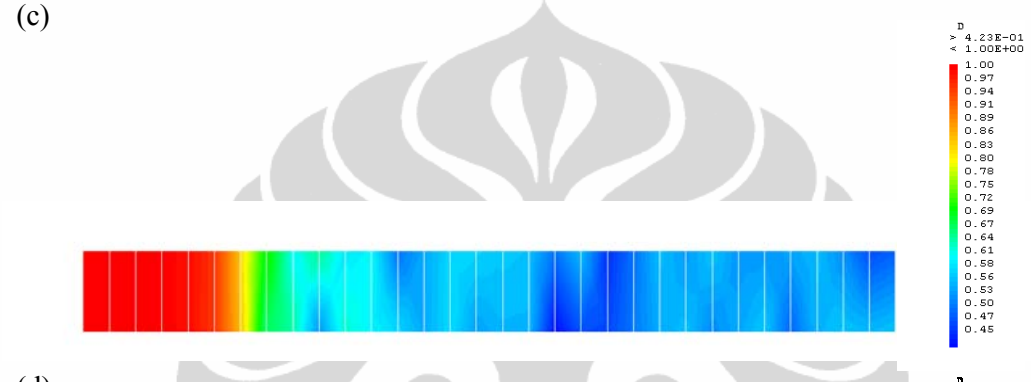

(d)

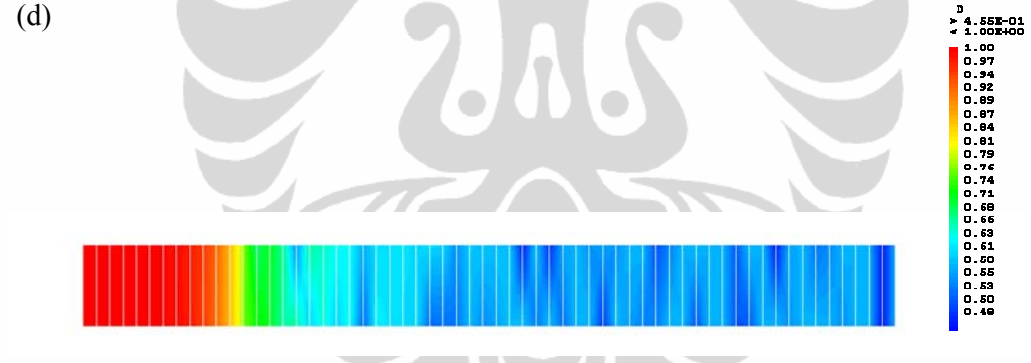

4.2 . THREE POINT BENDING TEST

4.2. 1. Model Definition

The experimental three point bending test of concrete beams has been done by SYED Yasir - Alam (2009) in research of scaling problem. In this section, a numerical three point bending calculation of notched concrete beam will be done. The beams are subjected by a concentrated vertical load *F* in the centre of the beam, and it is pin – roll supported at the bottom edge of the beam. Calculations are driven by plane stress and three different sizes of beams are to be calculated, where characteristic size may be seen in table 4.2.1.

Table 4.2. 1. Characteristic size for each specimen

Specimen	Length	Height	Notch thickness	Notch length	Support location
D1	L/2	h/2	0.00175	h/5	s/2
D2	L	H	0.00175	h/5	s
D3	2L	2h	0.00175	h/5	2s

where L is 0,8m, h is 0,4*m* and s is 0,1*m*. For the reason of simplicity, only half of the beam will be modeled as shown in figure 4.2.1.

Figure 4.2. 1. Size model of the beams (a) D3, (b) D2, (c) D1

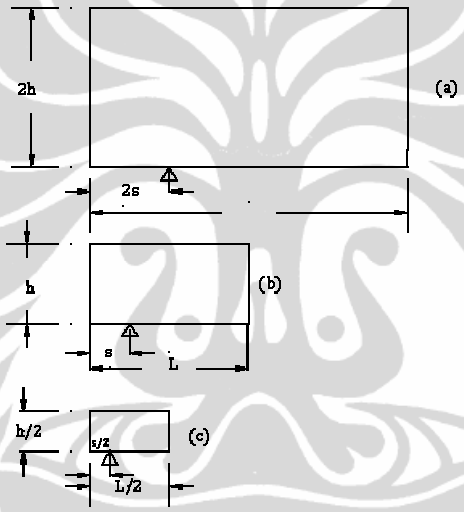

The material parameters used are

- Young Modulus $E = 30 \times 10^9\ N/m^2$
- Tensile strength $f_t = 1{,}65 \times 10^6\ N/m^2$
- Damage threshold $\varepsilon_{DO} = 5{,}5 \times 10^{-4}$
- Poisson ratio $\upsilon = 0{,}25$

Figure 4.2. 2. Modeling of the beam and the mesh refinement of D1 (a), D2 (b), D3 (c)

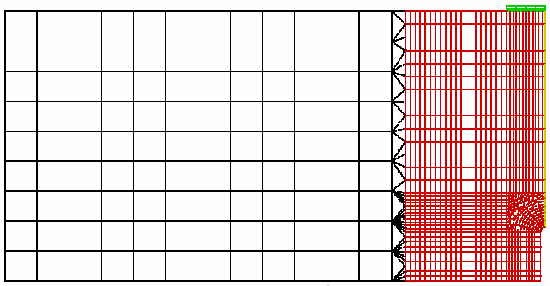

(a)

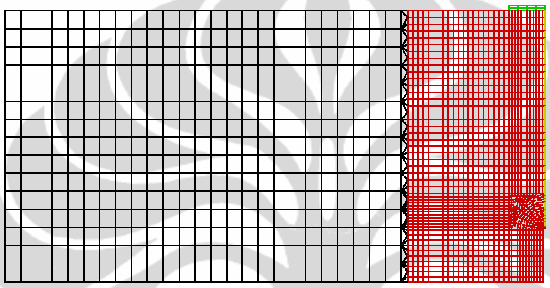

(b)

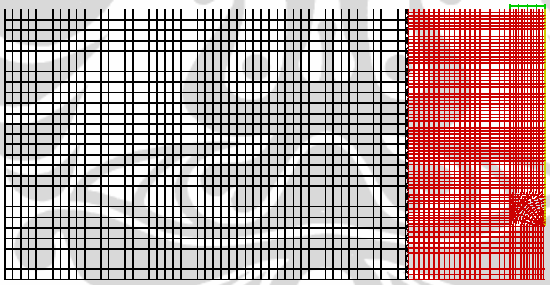

(c)

4.2. 2. Local Calculation

The local calculation is derived in order to see how the structure behaves in a local damage law. The concrete beam is modeled by Mazars damage model with standard parameters. Figure 4.2.3 shows the Force - Crack Opening Displacement (COD) for each type of beam, compared with the experimental result.

Figure 4.2. 3. Force – COD curve of local calculation

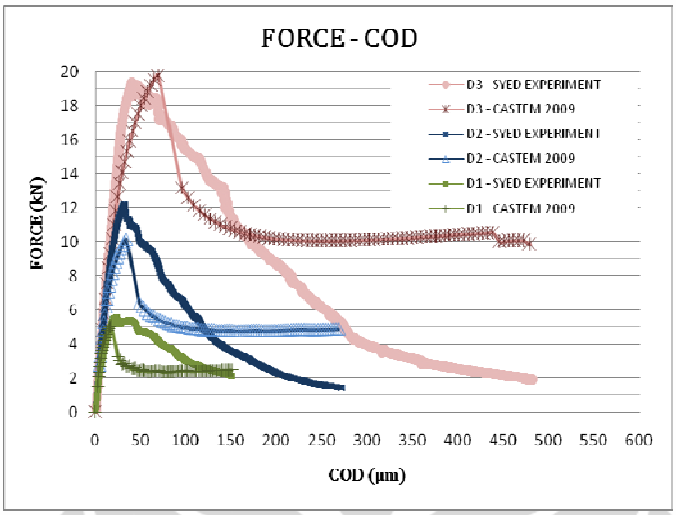

From figure above, it is shown that the numerical result and the experiment result are different. However, this is expected, since the parameters used for the numerical calculation is not calibrated from the experimental result.

Figure 4.2.4 – 4.2.6 shows the crack opening of the beam in order to see how the beam behaves locally. It shows that the crack propagates following the mesh refinement, where this result shows that the local behavior depends on the mesh refinement.

Figure 4.2. 4. Damage field D1 at final state, local calculation

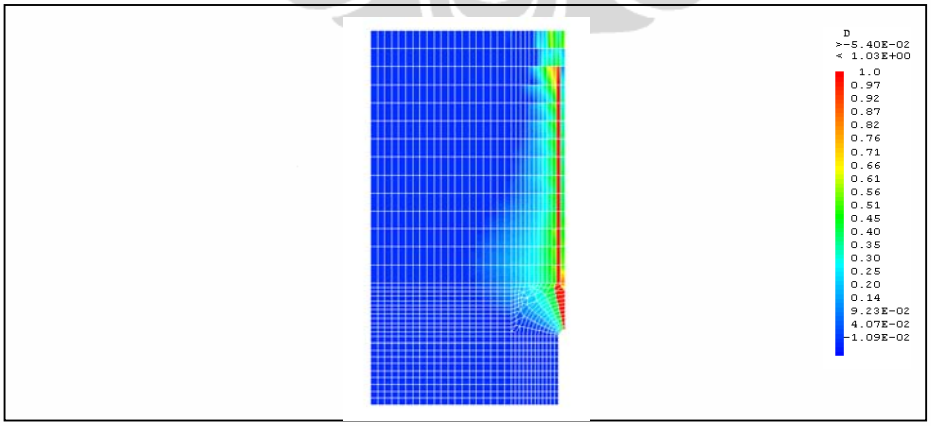

Figure 4.2. 5. Damage field D2 at final state, local calculation

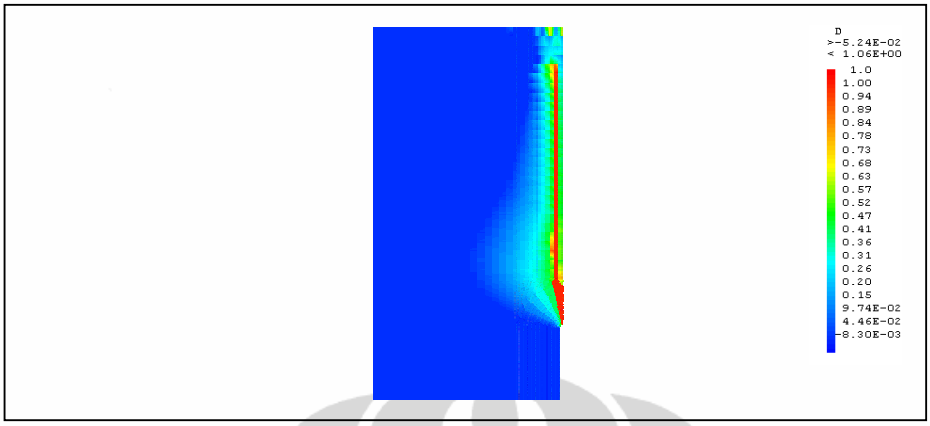

Figure 4.2. 6. Damage field D3 at final state, local calculation

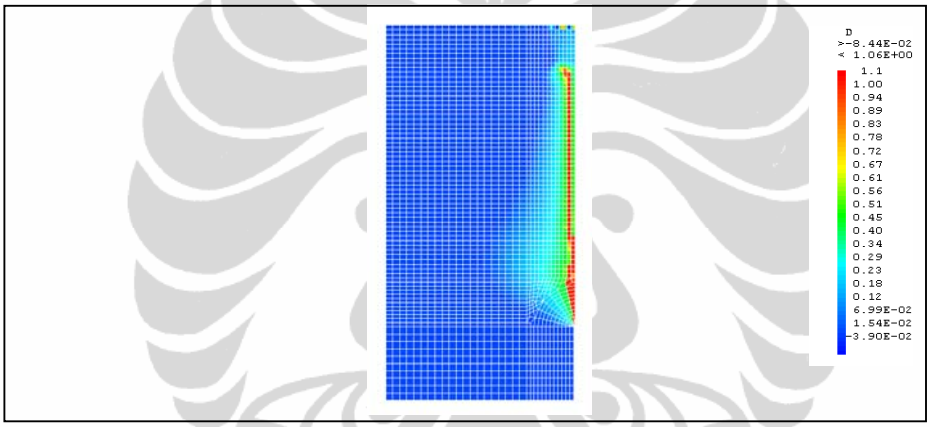

4.2. 3. Non Local Calculation

To overcome the mesh dependency, another calculation to be derived is the non - local calculation. The concrete beam is modeled by Mazars damage model with parameters given by SYED Yasir Alam (2009) based on the experimental result. These parameters (shown in table 4.2.2) are obtained by calibrating the experimental result of Force – Crack Opening Displacement (COD) curve of D2, from 60% before peak load until 60% after peak load.

Table 4.2. 2. Mazars damage parameters for non local calculation

At	Bt	Ac	Bc	β	Lc
0,731	8668,7	1.2	30 × 103	1.06	3,49

Global Result

Figure 4.2.7 shows the Force – COD curve obtained from each different size of beam. The size effect can be seen, where as the beam size is increased, the peak load also increases. Also in figure 4.2.7, a comparison of numerical result and experimental result obtained by SYED Yasir Alam (2009) is presented.

It can be seen that for D2, the Force - COD curve by numerical calculation gives almost the same curve as the experimental one, until a certain point where it differs; this is the point where the calibration was not taken into account. The maximum force of D2 given by numerical calculation is 12,20*kN* while the experimental gives 12,25*kN*, thus 2,24% of relative error. For D1, one may see that the numerical calculation gives a different Force – COD curve from the experimental result. The peak load from the numerical result is 7,80*kN*, while the experimental result is 5,546*kN*, which gives 40,6% of relative error. Meanwhile, for D3, the numerical result of Force – COD displacement is almost the same with the experimental result, where for the numerical result, the peak load is 17,8*kN* while the experimental test gives 19,33*kN*, which gives a relative error of 7,92%

Figure 4.2. 7. Force – COD curve, non local calculation

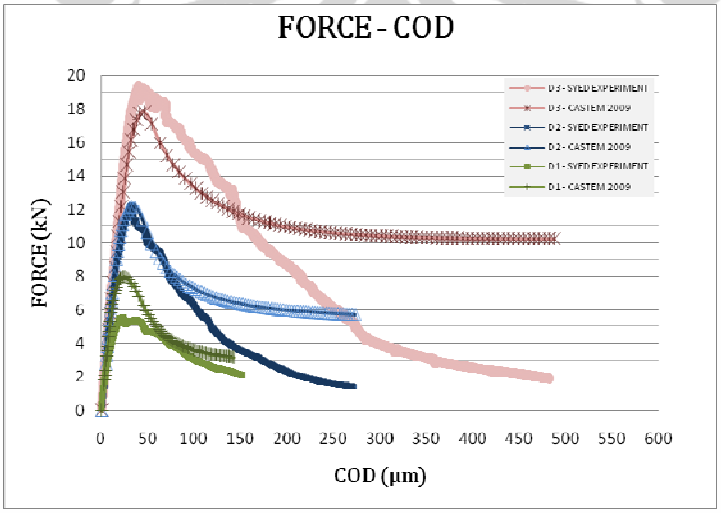

Damage Field

Figure 4.2.8 – 4.2.10 show the field of the beam.

Figure 4.2. 8. Damage field D1 at final state, non local calculation

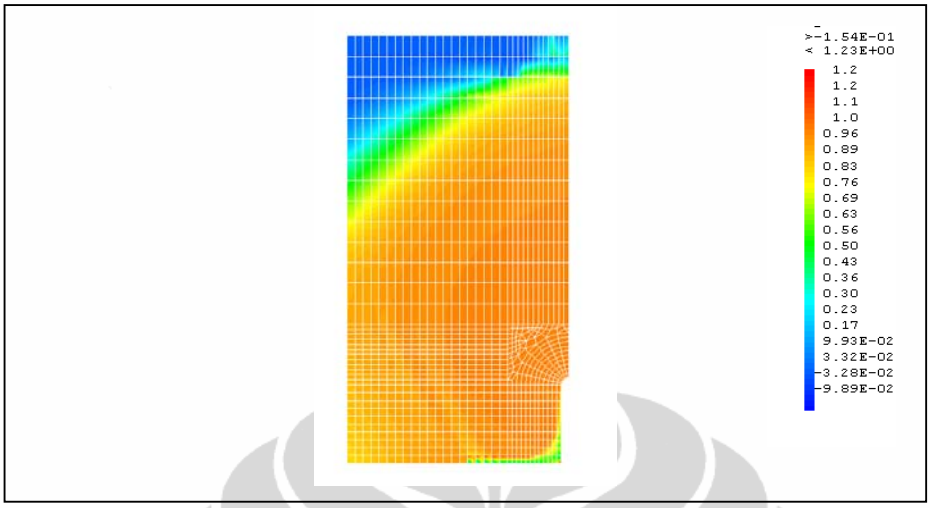

Figure 4.2. 9. Damage field D2 at final state, non local calculation

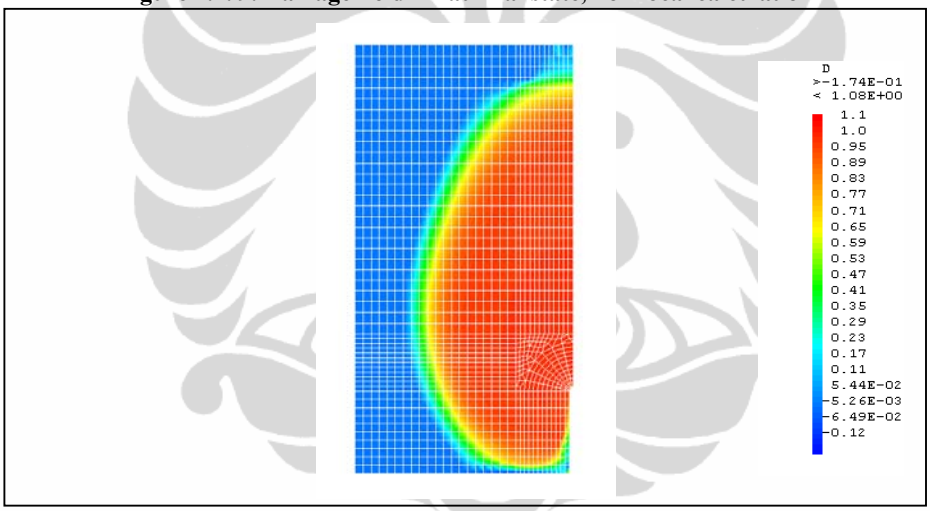

Figure 4.2. 10. Damage field D3 at final state, non local calculation

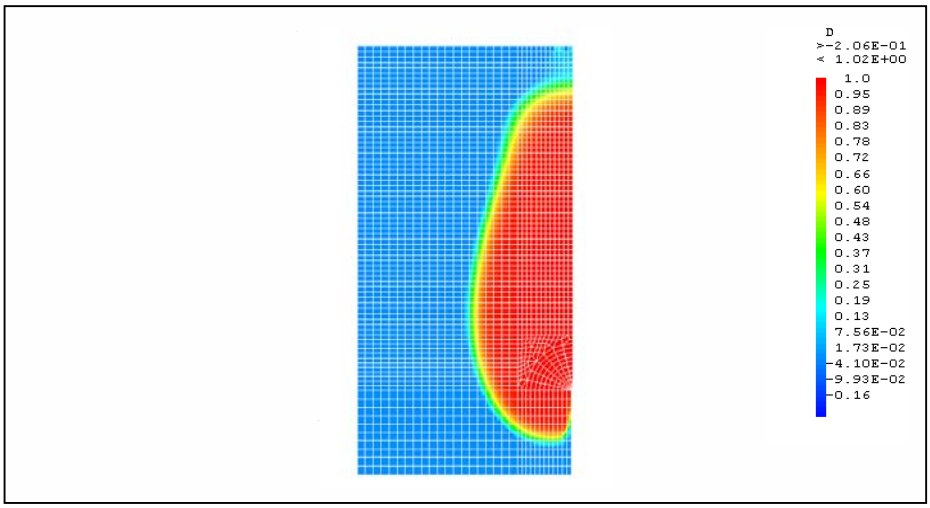

As the *Lc* parameter is the same for every size of beam, therefore, it is obvious that the damage area at D1 seems to be very large while the damage area at D3 does not seem to be as large, regarding to its total area. However, damage is actually occurred in a specific area that has been determined before by the localization limiters *Lc*. Therefore, the localization limiter is able to overcome the problem of mesh dependency in local behavior.

Crack Length and Crack Opening Displacement

Besides regarding at the global result, it is also necessary to look at the local result, which may be given by the crack opening displacement (COD), since crack is the one of the essential parameter in order to study the strength behavior of a structure. As mentioned before that the damage parameters were calibrated by considering the COD, therefore, another value is needed in order to verify the accuracy of the calibration. One may consider the crack length as the suitable value, because the propagation of crack length is related to one of COD.

Figure 4.2.11 – 4.2.13 show the curve of COD vs. crack length of the experimental result and the numerical result (where the numerical calculation, it uses the height of the beam as parameter of the crack length) at 60% before the peak load, at peak load, and at 60% after the peak load.

Figure 4.2. 11. Crack length – crack opening curve, D1, non local calculation

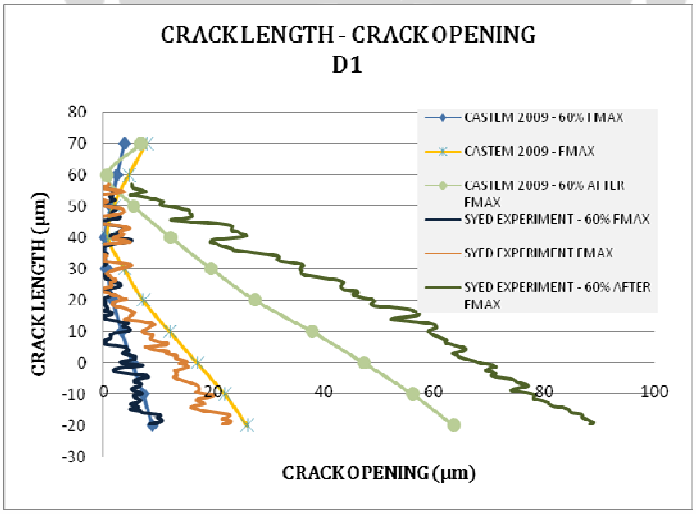

Figure 4.2. 12. Crack length – crack opening curve, D2, non local calculation

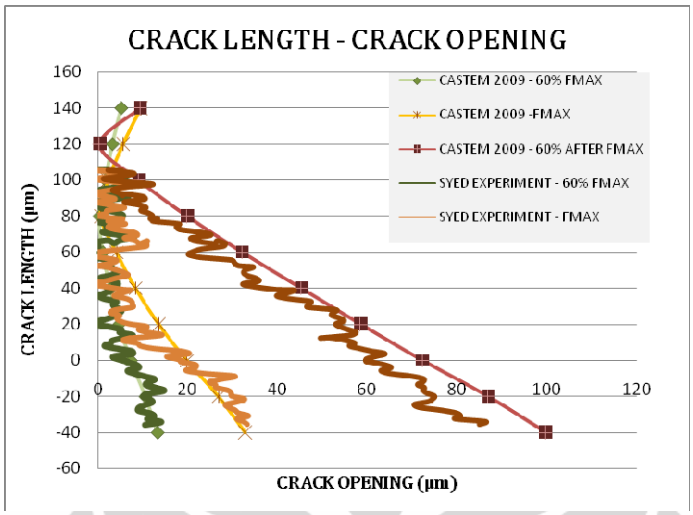

Figure 4.2. 13. Crack length – crack opening curve, D3, non local calculation

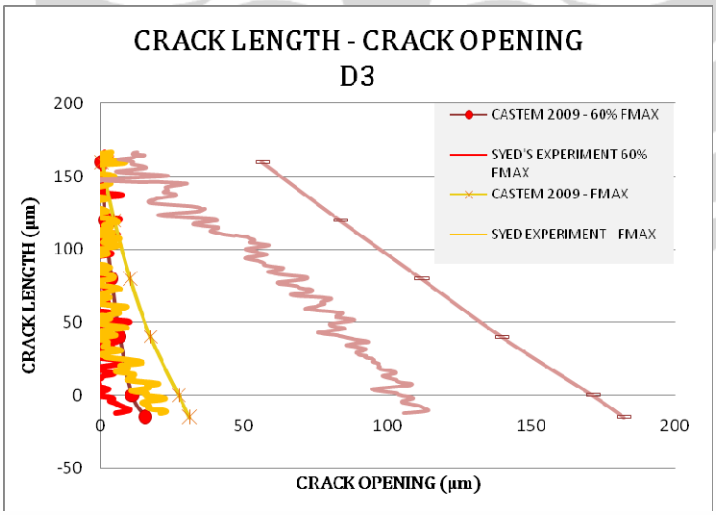

Table 4.2. 3. Quantification of relative error in COD

COD (µm)		60% before Peak Load		Peak Load		60% after Peak Load	
		Numeric	Experiment	Numeric	Experiment	Numeric	Experiment
D1	COD	5,26	3,38	17,02	14,90	47,30	68,62
	%RE	**55,84**		**20,76**		**31,07**	
D2	COD	7,29	4,55	19,78	17,60	72,28	59,72
	%RE	**60,28**		**12,41**		**21,04**	
D3	COD	11,02	1,26	27,37	15,94	171,47	105.1
	%RE	**777,1**		**71,68**		**63,15**	

Table 4.2. 4. Quantification of relative error in crack length

CL (μm)		60% before Peak Load		Peak Load		60% after Peak Load	
		Numeric	Experiment	Numeric	Experiment	Numeric	Experiment
D1	CL	40	55,85	45	55,70	60	57,28
	%RE	28,39		19,21		4,74	
D2	CL	80	105,36	90	105,36	120	105,36
	%RE	24,07		14,58		13,90	
D3	CL	160	166,84	160	166,84	160	166,84
	%RE	4,10		4,10		4,10	

Regarding to figure 4.2.11 – 4.2.13, one may see that the crack length measured numerically and experimentally gives almost the same result. However for the crack opening, there are some significant relative errors. Table 4.2.3 and 4.2.4 show the quantification of relative errors between the value of COD and crack length computed by numerical calculation and one by experiment. Measurements are done in certain step of load, which are 60% before peak, at peak load, and 60% after the peak load. It is shown that the numerical values overestimate the experimental value. However, numerical values are computed using the displacement jump, therefore such relative errors are expected.

CHAPTER 5
CONCLUSION

5. 1. CONCLUSION

From the numerical calculation that has been done, here are the conclusions:

5.1. 1. One Dimensional Uniaxial Calculation

A numerical calculation of one dimensional uniaxial concrete bar has been done. The bar is subjected to a load in the *x* direction and is computed as a plane stress. There are four types of mesh refinement, e.g. 11, 21, 31 and 61 meshes in order to see the mesh – independence in numerical calculation. Beam is given a weak area since continuum damage models need a point for crack initiation.

1. Local Calculation

   In doing a local numerical calculation, a result with mesh dependency will occur. The force – displacement graph obtained is affected by the mesh refinement; the graph behavior will be more brittle as the mesh being refined. Therefore the objectivity aspect is not fulfilled. To overcome this problem, a regularization numerical method is needed,

2. Hillerborg Approach using Mazars Damage Law

   One of the regularization numerical methods is by implementing the Hillerborg approach into the Mazars Damage Law. Two tension parameters can be obtained in order to implement the approach, e.g A_t and Bt. Mazar's tension parameter B_t gives an influence to the peak value of stress – strain graph thus an accurate result will not be obtained. For an approach using A_t, a suitable value of A_t cannot be obtained, since the values are less than 0 while A_t ranges from 0 to 1.

   Hence, Mazars damage law is not capable to be used in Hillerborg approach.

3. Hillerborg Approach using Evolution Damage Law by La Borderie

   An evolution damage law has been conducted by La Borderie. The B_t values are obtain and implemented in the calculation. A mesh independent

force – displacement curve is obtained. Meanwhile when the local behavior is observed, it gives a mesh – dependency result. Therefore, the La Borderie law may give good mesh independency result globally, but not in the local result.

4. Non Local Damage Law

   Another approach to overcome mesh dependency is to use a non local method, by implementing a localization limiter. A calculation hindrance occurred due to the lack of CAST3M capability in defining the connectivity between two different types of material, thus a localization limiters is not applicable in calculating one dimension bar with weak area.

5. Non Local Damage Law with Random Property Method

   The idea of this approach is to deal with the problem of predicting the crack position and number. The force – displacement curve obtained shows a mesh independency result. When the local behavior is observed, it is shown that the calculation is mesh independent. Therefore, the random property method is capable in giving a mesh – independent result globally and locally.

5.1. 2. Three Point Bending Test

A numerical three point bending test of concrete beam has been done. The beam is pin and roll supported on the bottom part of the beam and it is subjected to a concentrated load (–y direction) in the centre of the beam. There are three types of size of the beam to be analyzed, D1, D2, and D3, in order to simulate the size effect of the structures. Calculation is done by using Mazars Damage Law, therefore a notch is given at the bottom center of the, since the damage law needs point for crack initiation.

1. Local Calculation with

   The force - displacement curves vary for each type of beam as the size effect occurs, however the results obtained are not comparable with the experimental result, since the parameters of damage law used are different.

   For the local behavior, cracks occur along the mesh alongside the symmetric line according to the mesh refinement. Therefore, the local behavior is mesh dependant.

2. Non Local Calculation

Non Local Mazars damage parameters given are calibrated from the experimental results of SYED Yasir Alam (2009). The force – displacement curves given by each type of beam simulate the size effect, therefore for the global result, the regularization of numerical methods is able to simulate the size effect.

At the local behavior, crack length and crack opening are measured and compared with the experimental result. Values compared are ones at 60% before peak, at peak load, and 60% after the peak load. Given in table 4.2.3 and 4.2.4, the numerical results are overestimate compared to the experimental result, where relative errors which occur should be considered. However, the numerical results are computed using displacement jump, therefore another approach in calculating the crack opening displacement in order to obtain a more precise value that is comparable with the experimental results.

REFERENCE

[1] Mazars J. (1984). “Application de la mécanique de l’endommagement au comportement non linéaire et à la rupture du béton de structure”. Thèse de doctorat d’état de l’Université Paris VI.

[2] Lemaitre J. et Chaboche J.L. (1988). Mécanique des matériaux solides. Ed. Dunod.

[3] Baz˘ant, Z. P., Scaling of Structural Strength, Hermes-Penton, London, 2002.

[4] Ba ant ZP. Instability, ductility, and size effect in strain-softening concrete. J Engng Mech Div, Am Soc Civil Engrs 1976;102(EM2):331–44; Disc. 103:357–8, 775–7; 104:501–2.

[5] Ba ant ZP. Fracture in concrete and reinforced concrete. In: Ba ant ZP, editor. Preprints, IUTAM Prager Symposium on Mechanics of Geomaterials: Rocks, Concretes, Soils, Northwestern University, Evanston. 1983. p. 281–316

[6] Ba ant ZP. Crack band model for fracture of geomaterials. In: Eisenstein Z, editor. Proceedings of the 4th International Conference on Numerical Methods in Geomechanics, vol. 3, Edmonton, Alberta. 1982. p. 1137–52

[7] M. Matallah, C. La Borderie, and O. Maurel. A practical method to estimate crack openings in concrete structures. Int. J. Nume. Analy. Meth. Geomechanics, Accepted.

[8] A. HILLERBORG, Analysis of fracture by means of the fictitious crack model particularly for fibre reinforced concrete, Int. Journal of Cement Composites, 2, 1980, pp. 177-184.

[9] Ngo D., Scordelis A.C., "Finite element analysis of reinforced concrete beams", *J. Am. Concrete Inst.* 64(14), 152-163 (1967)

[10] Rashid Y.R., "Analysis of prestressed concrete pressure vessels", *Nuclear Engng. and Design* 7(4), 334-344 (1968)

[11] Bazant Z.P., Oh B.H., "Crack band theory for fracture of concrete", *Materials and Structures,* RILEM, 16(93), 155-177 (1983a)

[12] Mendess S., Diamond S. – *A preliminary SEM study of crack propagation on mortar,* Cement and Concrete Research, Vol 10, 1980, pp 509-519.

[13] Peterson P. E –*Fracture energy of concrete : Method of determination*, Cement and Concrete Research, Vol 10. 1980, pp 78-89, and “Fracture Energy of Concrete : Practical Performance and Experimental Results,” Cement and Concrete Research, Vol 10, 1980, pp 91 – 101.

[14] Z.P. Bazant, J. Planas, Fracture and Size Effect in Concrete and Other Quasibrittle Materials, CRC Press, Boca Raton, Florida,1998.

[15] Baz˘ant, Z. P., Scaling of Structural Strength, Hermes-Penton, London, 2002.

[16] Baz˘ant, Z. P (1984). Size Effect in Blunt Fracture : Concrete, Rock, Metal. *J.Eng Mech* **110**, 518 – 535.

[17] Mazars J. (1984). “Application de la mécanique de l’endommagement au comportement non linéaire et à la rupture du béton de structure”. Thèse de doctorat d’état de l’Université Paris VI.

[18] Lemaitre J. et Chaboche J.L. (1988). Mécanique des matériaux solides. Ed. Dunod.

[19] Hillerborg, A., Modeer, M., and Peterson, P.E. (1076). “Analysis of crack formation and crack growth in concrete by means of fracture mechanics and finite elements”. *Cement and Concrete Research*, 6(6). 773 - 782

[20] M. Matallah, C. La Borderie, and O. Maurel. A practical method to estimate crack openings in concrete structures. Int. J.Nume. Analy. Meth. Geomechanics, Accepted.

[21] Ba˘zant Z, Oh B. Microplan model for progressive fracture of concrete and rock. *ASCE Journal of Engineering Mechanics* 1985; **11**:559–582.

[22] Matallah M, La Borderie C. Inelasticity – damage-based model to numerical modelling of concrete cracking. *Engineering fracture Mechanics* 2009; **76**(8) : 1087 – 1108.